What caused record-breaking aerosol loading over the South China Sea in April 2023

Saginela Ravindra Babu[1*] and Neng-Huei Lin[1,2*]

[1]Department of Atmospheric Sciences, National Central University, Taoyuan 32001, Taiwan.

[2]Center for Environmental Monitoring and Technology, National Central University, Taoyuan 32001, Taiwan.

Correspondence to**:** S. Ravindra Babu (baburavindra595@gmail.com) and Neng-Huei Lin (nhlin@cc.ncu.edu.tw).

Abstract:

In April 2023, the South China Sea (SCS) experienced an unprecedented surge in aerosol loading, with aerosol optical depth (AOD) reaching the highest levels recorded during the 2-decade period of Moderate Resolution Imaging Spectroradiometer (MODIS) satellite data ~~in the two-decade Moderate Resolution Imaging Spectroradiometer (MODIS) satellite data period~~ (2003–2023). AOD increased by ~150% relative to the long-term mean (2002-2022), indicating an anomaly exceeding 4σ, and was accompanied by pronounced enhancement in carbon monoxide (CO) at 700 and 500 hPa. Using multi-sensor satellite measurements and MERRA-2 reanalysis, we investigated the sources, driving mechanisms, and atmospheric dynamics behind this extreme aerosol event. MODIS fire counts, burned-area data, and NOAA HYSPLIT back-trajectory analyses identify intense biomass-burning (BB) across northern Peninsular Southeast Asia (PSEA) as the dominant source, particularly from Laos and Myanmar. The BB was facilitated by anomalous meteorological conditions associated with a persistent tropospheric anti-cyclonic anomaly over PSEA, which suppressed convection and promoted subsidence, elevated surface temperatures, and widespread drought. The dynamical large-scale circulation anomalies further revealed substantially altered transport pathways. A coupled dynamical pattern involving a western North Pacific (WNP) cyclone, a BoB anticyclone at 700 hPa, and a PSEA anticyclone at 500 hPa generated persistent northerly flow over the SCS, redirecting smoke plumes southward toward the SCS and southern BoB rather than along the climatological pathway toward Taiwan and the northwestern Pacific. These findings reveal how the combined influence of extreme BB emissions and anomalous circulation produced the record aerosol loading over the SCS,

highlighting critical links among BB emissions and atmospheric dynamics in shaping regional air quality extremes.

~~Satellite observations revealed a 150% increase in aerosol optical depth (AOD) from MODIS and a 50% rise in carbon monoxide (CO) at 700 and 500 hPa from Measurements Of Pollution In The Troposphere (MOPITT) over SCS. Here, we investigate the drivers and atmospheric mechanisms responsible for this extreme event, identifying large-scale biomass burning (BB) across northern Peninsular Southeast Asia (PSEA), particularly Laos and Myanmar as the primary source. Our analysis indicates that anomalously high surface temperatures, low soil moisture, reduced precipitation, and a persistent upper-tropospheric anticyclone created favorable BB conditions over PSEA. Laos alone accounted for ~56% of the BB activity in the region, recording its largest monthly burned area (1.08 million hectares) since 2002. Dynamical analysis of the large-scale atmospheric circulation patterns revealed a major shift in regional wind regimes: the climatological south-westerlies over the SCS were replaced by anomalous northerlies, driven by the eastward shift of the Bay of Bengal anticyclone and the development of a cyclone anomaly over the western North Pacific (WNP). These changes redirected smoke transport from the usual WNP pathway to the SCS, resulting in significant transboundary pollution. This study highlights the critical role of compound meteorological extremes and circulation anomalies in amplifying regional aerosol loading, with implications for air quality, climate feedbacks, and environmental monitoring across Southeast Asia.~~

Key words: Aerosol loading; South China Sea; MODIS; ~~Wildfires~~Biomass burning

1. Introduction

Atmospheric aerosols play a vital role in Earth's climate by impacting radiation balance, cloud microphysics, and air quality (Ramanathan et al., 2001; Anderson et al., 2003; Forster et al., 2021; IPCC, 2023). These particles scatter and absorb solar radiation directly, influencing radiative effects, and also modify cloud properties, lifespan, and precipitation by serving as nuclei for condensation and ice formation. As a result, aerosols affect atmospheric thermodynamics, cloud–radiation interactions, and the water cycle (Twomey et al., 1977; IPCC, 2023). Monitoring aerosol levels over remote ocean regions is especially important because these areas provide a baseline for natural background aerosol levels and help evaluate the effects of long-range transport and their influence on regional climate through radiative and cloud processes (Pani et al., 2023). In addition

to anthropogenic emissions, natural events such as wildfires and agricultural biomass burning are significant episodic sources, emitting large quantities of aerosol particles and trace gases that substantially affect both regional and global climate systems (Crutzen and Andreae, 1990; Ramanathan et al., 2001; Lin et al., 2013; Reid et al., 2013; Kolden et al., 2024).

The South China Sea (SCS), situated in Asia, is the largest marginal sea in the tropical–subtropical western North Pacific, serving as a vital natural laboratory for examining aerosol variability in a relatively pristine marine environment (Reid et al., 2013; Lin et al., 2013; Pani et al., 2023). Although it is an oceanic region, the atmosphere over the SCS is significantly influenced by emissions from nearby continents and regional circulation patterns (Pani et al., 2023). Typically, the SCS is dominated by a monsoon system, with the northeast monsoon occurring during boreal winter and spring, and the southwest monsoon during boreal summer and autumn (Cui et al., 2016). These seasonal wind patterns play a key role in aerosol transport, often carrying natural and human-made pollutants from East Asia into the SCS basin over long distances. In addition to continental outflow from East Asia, biomass-burning emissions from surrounding areas notably influence aerosol concentrations over the SCS. During the summer monsoon months, particularly August to October, persistent peatland and forest fires across the Maritime Continent (MC) generate large smoke plumes that drift toward the southern SCS (Ravindra Babu et al., 2023). Moreover, extensive open biomass burning in spring over Peninsular Southeast Asia (PSEA), including Myanmar, Thailand, Cambodia, Laos, and Vietnam, serves as a key source of aerosols affecting the SCS atmosphere (Chan et al., 2003; Ou-Yang et al., 2012; Yadav et al., 2017; Liao et al., 2021; Wang et al., 2021; Pani et al., 2023; Wang et al., 2025). This region is recognized as a global hotspot for biomass burning (Lin et al., 2013; Reid et al., 2013; Cohen, 2014; Cohen et al., 2017; Pani et al., 2019), significantly contributing to carbon emissions and aerosol loading during the peak fire season in March and April (Ravindra Babu and Lin, 2023). These fires mainly stem from slash-and-burn farming practices occurring annually across PSEA (Lee et al., 2016; Tsay et al., 2016; Huang et al., 2020), releasing substantial particulate matter and trace gases into the air (Ou-Yang et al., 2022). As a result, aerosol variability in the SCS region is largely driven by the interaction between regional emission sources and the prevailing monsoon circulation, which influences aerosol transport, dispersion, and accumulation within the basin (Pani et al., 2023).

The year 2023 saw exceptional wildfires worldwide due to record-high global mean surface temperatures, which affected carbon emissions and aerosol levels (Esper et al., 2024; Forster et al., 2024; Min, 2024; Raghuraman et al., 2024; Kolden et al., 2024; Liu et al., 2024; Byrne et al., 2024; MacCarthy et al., 2024). It is reported that 70% of the total burning occurs in the Northern Hemisphere (Kolden et al., 2024). Among all, Canadian wildfires emerged as the primary hotspot, with significant fires in both the eastern and western regions causing notable increases in carbon monoxide (CO) and tropospheric aerosols over the past twenty years (Liu et al., 2024; Byrne et al., 2024; MacCarthy et al., 2024). Although the unprecedented Canadian wildfires in 2023 received considerable scientific attention and were well documented in several studies, the record-breaking aerosol loading over the SCS in April 2023 attracted relatively little international attention. The historic event over the SCS in April 2023 can be seen through the Moderate Resolution Imaging Spectroradiometer (MODIS) Aqua AOD anomalies compared to the long-term mean (2003-2022), which shows extreme positive anomalies over the SCS and surrounding regions during that month, contrasting with the rest of the globe (**Fig. 1**). However, AOD anomalies in May illustrate the absence of positive anomalies over the SCS and instead show higher positive anomalies over North America, which are related to the Canadian wildfires. The time series of monthly mean AOD over the SCS further confirms a record-high AOD in April 2023 relative to the MODIS data from 2003 to 2023 (**Fig. 2d**). The exceptional aerosol loading in April 2023 is unusual for remote marine locations such as the SCS and warrants further investigation. In this study, we investigated the factors and physical processes that contributed to the unprecedented aerosol levels observed in April 2023, using extensive data collected from multiple sources over an extended period. The following three major topics are examined in detail within this study:~~In the changing climate scenario, both natural and anthropogenic activities have contributed to a continuous increase in surface temperatures worldwide over the past decade (Seneviratne et al., 2021). In 2023, a record-high global mean surface temperature was observed, marking the warmest period in the last seven months (June to December), surpassing the previous record set in 2016 by a significant margin of 0.13°C to 0.17°C (Esper et al., 2024; Forster et al., 2024; Min, 2024; Raghuraman et al., 2024). The extreme temperatures contributed to record-breaking wildfires worldwide in 2023, with 70% of the total burning occurring in the Northern Hemisphere (Kolden et al., 2024). Among all, Canadian wildfires emerged as the primary hotspot in 2023, with significant fires in both the eastern and western regions causing notable increases in~~

carbon monoxide (CO) and tropospheric aerosols over the past twenty years (Liu et al., 2024). The unprecedented wildfire season in Canada from May to September 2023 burned three times more biomass than the previous record, leading to the highest annual carbon emissions from biomass burning (BB) since 2015 (Byrne et al., 2024; MacCarthy et al., 2024). Furthermore, catastrophic wildfires have also occurred in regions such as Hawaii, the Mediterranean, central Amazonia, and central Chile (Roy et al., 2024; Lemus‐Canovas et al., 2024; Espinoza et al., 2024; Jones et al., 2024; Cordero et al., 2024). Greece experienced its most severe wildfire on record, with a burned area of 96,000 hectares in 2023 (Michailidis et al., 2024). The August 2023 wildfires on Maui, Hawaii, were among the deadliest U.S. wildfire incidents, resulting in 100 deaths and an estimated loss of $5.5 billion (NOAA NCE, 2023). As a result of multiple fire spots across the globe, the global mean concentrations of atmospheric carbon dioxide (CO_2), methane (CH_4), and nitrous oxide (N_2O) reached new annual record highs of 419.3 ppm, 1922.6 ppb, and 336.7 ppb, respectively. The global atmospheric CO_2 growth rate in 2023 was 2.79 ± 0.08 ppm (Ke et al., 2024; Gui et al., 2024), the third largest since 2000 and the fourth largest since 1959.

The Asian region frequently experiences forest fires and biomass burning activities, significantly impacting the global carbon footprint (Xia et al., 2025). The South China Sea (SCS) in Asia is the largest marginal ocean region in the tropical–subtropical western North Pacific. It is a prime example of a marine area with minimal air pollution (Pani et al., 2023). This is further supported by long‐term satellite‐measured Aerosol Optical Depth (AOD) spatial distribution. **Sup. Figures 1a** and **1b** indicate shallow AOD values with minimal standard deviations in the SCS, illustrating a clean marine environment. The SCS has a monsoon climate characterized by a northeast monsoon during winter and spring and a southwest monsoon during summer and autumn (Cui et al., 2016). These monsoon circulations allow natural and anthropogenic pollutants from East Asia to be lifted and transported over long distances to the SCS (Lin et al., 2013). During the summer monsoon season (August and September), the frequent burning of peat forests on the Maritime Continent (MC) also affects the adjacent regions of the southern SCS. In addition to East Asia and the MC, the springtime open biomass burning (BB) over Peninsular Southeast Asia (PSEA, including Myanmar, Thailand, Cambodia, Laos, and Vietnam) also impacts the SCS. The PSEA is one of the hotspot regions with the most intensive biomass burning activities in the world (Lin et al., 2013; Reid et al., 2013) and is a major contributor to carbon emissions and atmospheric aerosols during the springtime (March–April). Open BB occurs almost every year during spring in

~~the PSEA due to slash-and-burn agricultural activities (Lee et al., 2016; Tsay et al., 2016; Huang et al., 2020), emitting a substantial number of aerosols and trace gases into the atmosphere (Ou-Yang et al., 2022). The influence of aerosol loading over the SCS is strongly associated with the sources of aerosols and the prevailing wind circulation.~~

~~Although the unprecedented Canadian wildfires in 2023 garnered immense scientific interest and were well-documented in several studies, the record-breaking aerosol loading in the SCS in April 2023 received relatively little international attention. The historic event over the SCS in April 2023 can be observed from the Moderate Resolution Imaging Spectroradiometer (MODIS) Aqua AOD anomalies compared to the long-term mean (2003-2022), which shows extreme positive anomalies over the SCS and surrounding regions in April 2023, in contrast to the rest of the globe (**Fig. 1**). However, AOD anomalies in May further illustrate the absence of positive anomalies over the SCS and the presence of higher positive anomalies specifically over North America, particularly Canada. The time series of monthly mean AOD over the SCS further indicates a record-high AOD in April 2023 compared to the rest of the MODIS data from 2003 to 2023 (**Sup. Fig. 2d**). The exceptional record-breaking aerosol loading in April 2023 is unusual for remote marine locations such as the SCS and requires detailed investigation. In this communication, we examine the factors and physical processes that contributed to the unprecedented aerosol levels observed in April 2023, utilizing extensive data collected from multiple sources over an extended period. The following three major topics are explored in detail in the present study:~~

- How extreme are these AOD~~/CO~~ anomalies, and what magnitude was increased?
- What are the sources for these record-breaking aerosol loadings over SCS?
- Were dynamic and large-scale circulations responsible for this event?

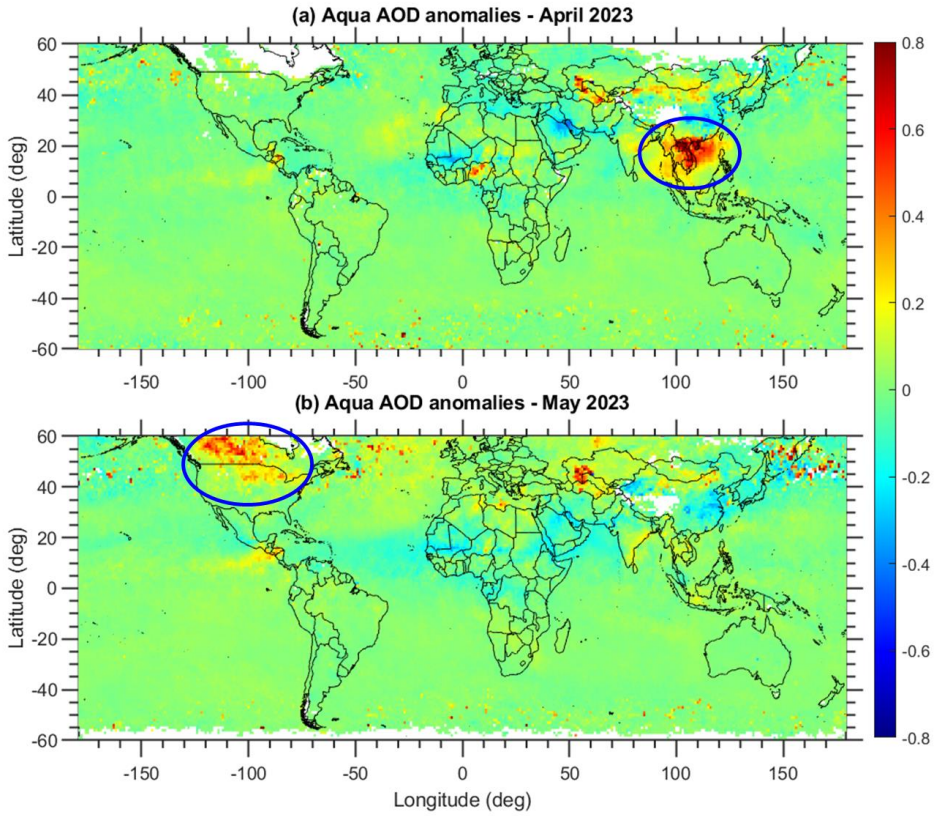

Figure 1. MODIS Aqua measured AOD anomalies in (a) April 2023 and (b) May 2023 compared to the long-term mean (2003-2022). The highlighted circles in (a) and (b) indicate the AOD anomalies over the South China Sea (SCS) and Canada regions. This figure highlights that the AOD anomalies observed by MODIS are significant and particularly pronounced over the SCS compared to the other areas globally. It illustrates the unique characteristics of April 2023 ~~in terms of~~compared to long-term mean ~~climatology~~. Data visualizations produced using MATLAB 2023b (https://matlab.mathworks.com).

2. Data and Methodology

2.1~~.1~~ Data

This study relies entirely on publicly available data, covering the period from 2003 to 2023. We used data products from various satellite measurements, ground-based observations, and reanalysis products. ~~For example, AOD data is obtained from MODIS, while CO data is obtained from MOPITT and AIRS satellites, respectively. The tropospheric column ozone data are obtained from OMI/MLS along with AIRS ozone data at 700 hPa and 500 hPa, respectively.~~

2.1.1 Satellite remote sensing measurements

Moderate Resolution Imaging Spectroradiometer (MODIS)

MODIS is a passive sensor aboard the Aqua and Terra satellites, which are in a sun-synchronous orbit, and pass the Equator in the morning (Aqua) and afternoon (Terra). From MODIS satellite measurements, we utilized aerosol optical depth (AOD), fire counts, fire radiative power (FRP), cloud fraction, and burned area products. We used Level 3 monthly AOD at $1^\circ \times 1^\circ$ spatial resolution derived from the mean of the Dark Target and Deep Blue Combined Aerosol Products from the Terra satellite (MOD08_M3 Collection 6.1) and Aqua satellite (MYD08_M3 Collection 6.1) (Platnick et al., 2015; Buchholz et al., 2020). For MODIS AOD, the estimated uncertainty is approximately ±0.05 over ocean and ±0.15 over land. The Collection 6.1 (C6.1) products used in this study have been shown to capture temporal variations effectively and agree closely with ground-based observations (Wei et al., 2019a). Validation against AErosol RObotic NETwork (AERONET) measurements demonstrates that the merged Dark Target and Deep Blue (DTB) products accurately capture aerosol variability at both regional and global scales (Sayer et al., 2014; Wei et al., 2019b). Additionally, we ~~utilized MODIS's product of daily fire counts and fire radiative power (FRP)~~ used MODIS's daily fire counts and fire radiative power (FRP) products (Giglio et al., 2006, 2016, 2018). Direct fire counts from MODIS were obtained from the Fire Information for Resource Management System (FIRMS) dataset. We selected all MODIS fire counts from the Terra and Aqua sensors with a confidence level of at least 80%. ~~or higher. Each month, the total MODIS daily fire counts and FRP are constructed and gridded at a resolution of 0.25° latitude × 0.25° longitude.~~ Finally, we utilized Cloud Fraction data from both the Terra and Aqua satellites.

Measurements Of Pollution In The Troposphere (MOPITT)

MOPITT is a multi-channel thermal infrared (TIR) and near-infrared (NIR) instrument operating on board the sun-synchronous polar-orbiting NASA Terra satellite. This study uses a version 9

(MOP03TM_9) gridded monthly product (Worden et al., 2010; Deeter et al., 2019). For more details ~~about~~ on the retrieval algorithm, validation, and uncertainties in MOPITT CO, ~~refer to~~see Deeter et al. (2019).

Atmospheric Infrared Sounder (AIRS)

In addition to the MOPITT measurements, we ~~utilized CO from the AIRS on the NASA Aqua satellite, which provides CO at different~~used CO from the AIRS instrument on the NASA Aqua satellite, which provides CO at multiple vertical levels twice daily and has near-global coverage. AIRS uses wavenumbers 2183–2200 cm−1 (4.58–4.5 µm) for retrieving CO (McMillan et al., 2005). The V9 level 3 CO product, available at 1° × 1° resolution at ~~various~~ 700 and 500 hPa~~pressure~~ levels, was utilized in the present study. AIRS sensitivity to CO is broad and optimal in the mid-troposphere between approximately 300 and 600 hPa (Warner et al., 2007, 2013; AIRS project, 2019). CO retrievals exhibit a 6%–10 % bias between 900 and 300 hPa with a root mean square error of 8%–12 % (McMillan et al., 2011). In addition to CO, we also utilized ozone, ~~skin~~ surface temperature, and outgoing longwave radiation (OLR) data from the AIRS satellite.

Formatted: Superscript

Formatted: Superscript

~~**Ozone Monitoring Instrument (OMI)/Microwave Limb Sounder (MLS)**~~

~~We utilized the OMI/MLS dataset of global tropospheric column ozone (TCO) concentrations, covering the period from 2005 to 2023, obtained from the Ozone Monitoring Instrument (OMI) and the Microwave Limb Sounder (MLS) (Ziemke et al., 2006). The total ozone column from OMI is derived using the Total Ozone Mapping Spectrometer (TOMS) version 8 algorithm. MLS measures vertical ozone profiles above the upper troposphere via limb scans ahead of the Aura satellite. TCO is then determined by subtracting MLS's stratospheric ozone measurements from OMI's total column ozone, after calibration adjustments between the two instruments via the convective-cloud-differential method (Ziemke et al., 2006). The OMI/MLS product provides monthly mean TCO data between 60°S and 60°N at a 1° × 1° resolution, starting from October 2004. This dataset has been extensively used to analyze global tropospheric ozone patterns (Ziemke et al., 2019; Cooper et al., 2010) and long-term trends (Gaudel et al., 2018; Lu et al., 2019).~~ **Global Precipitation Climatology Project (GPCP)**

The Global Precipitation Climatology Project (GPCP) Version 3.2 Satellite-Gauge (SG) Combined Precipitation Data Set was used during the study period. The data is available for

download from https://measures.gesdisc.eosdis.nasa.gov/data/GPCP/GPCPMON.3.2/ (last accessed June 5, 2025).

Cloud-Aerosol LIDAR with Orthogonal Polarization (CALIOP)

The CALIOP sensor on the Cloud-Aerosol Lidar and Infrared Pathfinder Satellite Observations (CALIPSO) satellite provides data on atmospheric aerosols, including aerosol layer heights and thicknesses, optical depth, aerosol type, and other optical properties (Omar et al.,2009; Kim et al., 2018). In our study, we used vertical aerosol-type images available on the CALIPSO website.

2..1.2 Reanalysis/model products

MERRA-2 reanalysis ~~products~~

We used monthly mean geopotential height, wind vectors (zonal and meridional wind speeds), and~~also utilized monthly mean geopotential height, wind vectors (zonal and meridional wind speed)~~, total column black carbon, organic carbon, and particulate matter from the Modern-Era Retrospective Analysis for Research and Applications, version 2 (MERRA-2). MERRA-2 is the latest atmospheric reanalysis data produced by the NASA Global Modeling and Assimilation Office (GMAO; Gelaro et al., 2017). The horizontal resolution of the MERRA-2 reanalysis is 0.5° × 0.625°.

Global Land Data Assimilation System (GLDAS)~~Soil Moisture~~

Monthly mean soil moisture content (10 - 40 cm underground) from the Global Land Data Assimilation System (GLDAS)_NOAH025_M v2.1 is utilized. The data can be downloaded from https://hydro1.gesdisc.eosdis.nasa.gov/data/GLDAS/GLDAS_NOAH025_M.2.1/ (last accessed: June 05, 2025).

2.1.3 Ground-based observations

AERONET

In this study, we use the latest version (V3) of Level 2.0 AERONET data from two stations: Dongsha Island (also called the Pratas Islands; Dongsha Island, 20.70°N, 116.73°E, 5 m above sea level) and Lulin Atmospheric Background Station (LABS, 23°28′N, 120°52′E, 2,862 m; Sheu et al., 2010). These offer cloud-screened, quality-checked direct-sun AOD retrievals with

uncertainties of about ±0.01 in the visible and ±0.02 in the ultraviolet range (Giles et al., 2019; Sinyuk et al., 2020).

The summary of the major data used in the present study is presented in **Table 1**.

Table 1. Details of various data products used in the present study.

Data	**Resolution**	**Source**
Aerosol Optical Depth (AOD)	1° × 1°	Aqua and Terra satellite/MODIS
Carbon Monoxide (CO)	1° × 1°	MOPITT and AIRS
Burned Area (BA)	500 m	Aqua and Terra satellite/MODIS
MODIS Collection 6.1 Fire Anomalies		combined Terra and Aqua satellite/MODIS
Wind and Geopotential Height	0.5° × 0.625°	MERRA reanalysis

Formatted Table

~~**Precipitation**~~

~~The Global Precipitation Climatology Project (GPCP) Version 3.2 Satellite-Gauge (SG) Combined Precipitation Data Set was used during the study period. The data is available for download from https://measures.gesdisc.eosdis.nasa.gov/data/GPCP/GPCPMON.3.2/ (last accessed June 5, 2025).~~

2.~~1.~~2 Methodology

The anomalies in the various parameters for April 2023 were estimated by subtracting the April background long-term mea ~~background long-term mean for April~~ (2003-2022) from ~~the value for~~ April 2023 value.

The magnitude of the AOD/CO enhancement in April 2023 above the long-term background was determined by comparing the average of April 2003-2022. We obtained the percentage change in AOD/CO relative to the respective background using Equation 1:

$$\text{Relative change in percentage} = \left(\frac{x_{i-\bar{x}}}{\bar{x}}\right) \times 100 \qquad \text{(Eq. 1)}$$

where x_i represents the monthly mean of April in 2023, and $\bar{x}$ is the long-term mean of April calculated using the data from 2003 to 2022.

3. Results and Discussion

3.1 Record-breaking aerosol loading ~~AOD and CO anomalies~~ over SCS in April 2023

Aerosol optical depth (AOD) is a common metric for measuring atmospheric aerosol loading and is crucial for radiative forcing assessments (Hirsch and Koren, 2021). In this study, we utilize AOD data retrieved from the MODIS instruments aboard the Aqua and Terra satellites for the period from 2003 to 2023. Before analyzing the unusual AOD conditions observed in April 2023, we first characterize the long-term AOD behavior over the study area using two decades of MODIS data. The spatial patterns of the long-term annual mean AOD and its associated standard deviation across the Asian region are shown in **Figures 2a** and **2b**, respectively. Additionally, the long-term monthly-mean variability of AOD over the two main biomass-burning (BB) regions surrounding the SCS, namely PSEA and the MC, is shown in **Figures 2c** and **2d**. The relatively low AOD levels and small standard deviations over the SCS suggest the dominance of a relatively clean marine environment. The seasonal cycle of AOD shows clear peaks linked to regional BB activities (**Figs. 2c** and **2d**). Over PSEA, AOD peaks during March–April, while over the MC, the peak occurs in September–October. These seasonal maxima align with well-known BB activity periods in these areas (Ravindra Babu and Lin, 2024; Chang et al., 2024). The fire season over the MC usually runs from August to October, whereas PSEA experiences intense BB activity from January to April, with a notable peak in March.

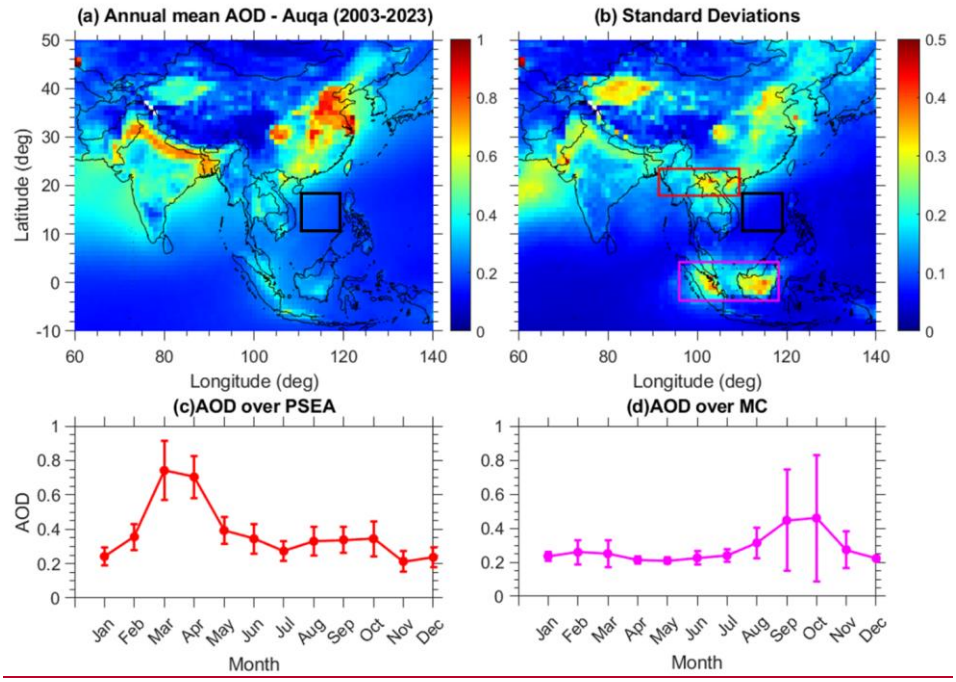

Figure 2. Climatological mean distribution of MODIS (a) Aerosol Optical Depth (AOD) and (b) respective standard deviations. The black box illustrated in both figures emphasizes the specific area of the South China Sea (SCS) that is the primary focus of this research. (109-119E, 11-18N). The red and magenta boxes indicate the PSEA and MC, two significant biomass-burning regions near the SCS. The long-term average seasonal variation in AOD is illustrated over (c) PSEA and (d) MC.

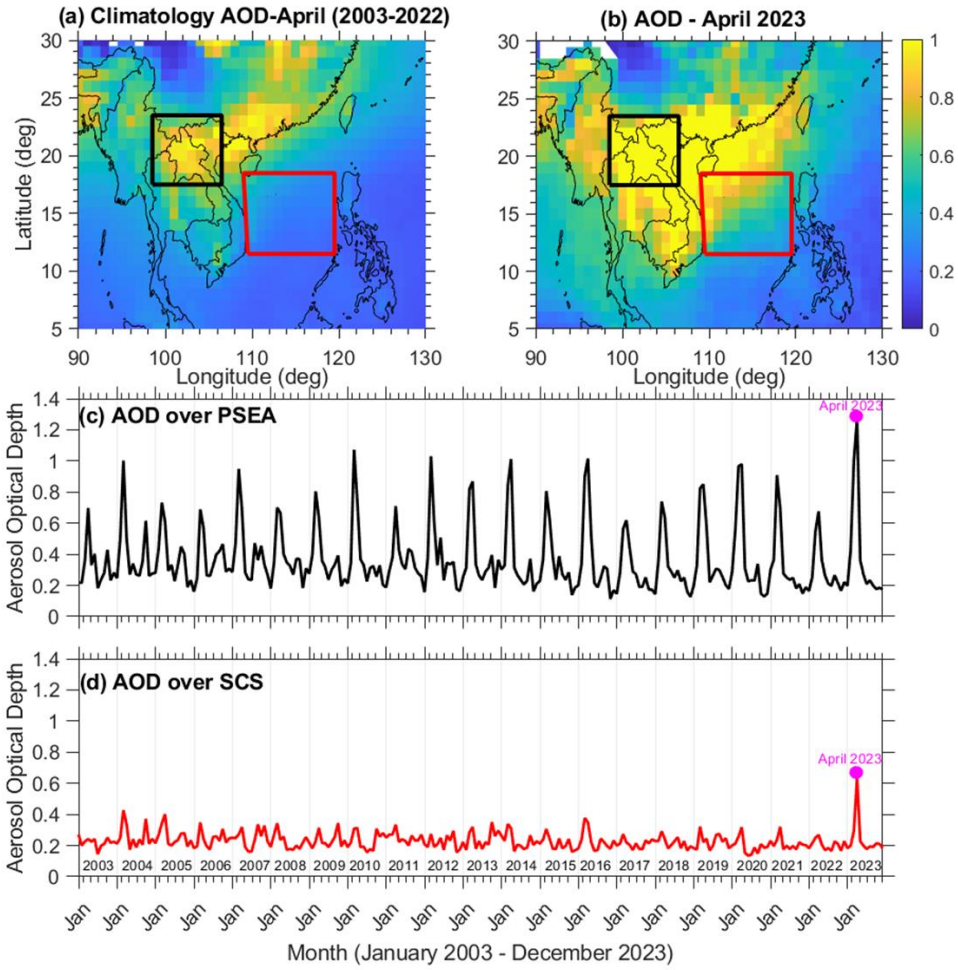

Figure 3. Spatial distribution of (a) Inter-annual (2003 to 2022) monthly average AOD values for April. (b) Monthly AOD values for April 2023. A notable increase in AOD values is observed over the peninsular Southeast Asia and the South China Sea. AOD distribution averaged in April over the past two decades showed a belt of high aerosol loading extending from northern Laos to the southern coast of China. During April 2023, extreme AOD values were observed across the entire PSEA, extending to coastal South China and the South China Sea. (c) Time series of average monthly mean AOD values over the northern Peninsula of Southeast Asia (17-23N, 99- 106E), and (d) over the South China Sea (109-119E, 11-18N) from January 2003 to December 2023. The magenta dot in subplots (c) and (d) marks the AOD values during April 2023.

To emphasize the anomalous conditions during April 2023, we present the spatial distribution of April AOD over the study region for both the long-term average and April 2023 specifically. The long-term average April AOD for 2003–2022 and the corresponding April 2023 AOD distribution are shown in **Figures 3a** and **3b**. Moreover, the time series of monthly mean AOD from 2003 to 2023 over northern PSEA (17–23°N, 99–106°E) and the SCS (11–18°N, 109–119°E) are displayed in **Figures 3c** and **3d**. The AOD distribution in April over two decades indicates high aerosol loading from northern Laos to coastal South China (15-25 N, 100-120 E). In April 2023, extreme AOD values extended from PSEA to South China and SCS, with the highest center between northern Laos and the SCS. Record-breaking AOD levels were observed for the area averaged over the SCS in April 2023, showing a nominal increase in northern PSEA (**Fig. 3c**). However, the highest AOD value for northern PSEA in April 2023 correlates with record AOD over the SCS. Long-term monthly mean AOD from Aqua and Terra (2003–2023) exhibited a strong correlation of 0.97, confirming the consistency and reliability of these observations (**Fig. S1a** in the Supplement). To assess the magnitude of the increase, we estimated the percentage change in AOD by comparing April 2023 with the long-term average for April from 2003 to 2022.

~~Aerosol optical depth (AOD) is a standard measure used to estimate aerosol loading and is a key parameter in calculating radiative effects. We utilize AOD data from MODIS instruments on the Aqua and Terra satellites from 2003 to 2023. **Sup. Figures 2a** and **2b** show the long-term (2003-2022) average AOD for April and the monthly mean AOD for April 2023. Time series of average monthly AOD values over northern PSEA (17-23 N, 99-106 E) and SCS (109-119 E, 11-18 N) from 2003 to 2023 are shown in **Sup. Figures 2c** and **2d**.~~

Formatted: Font: Bold

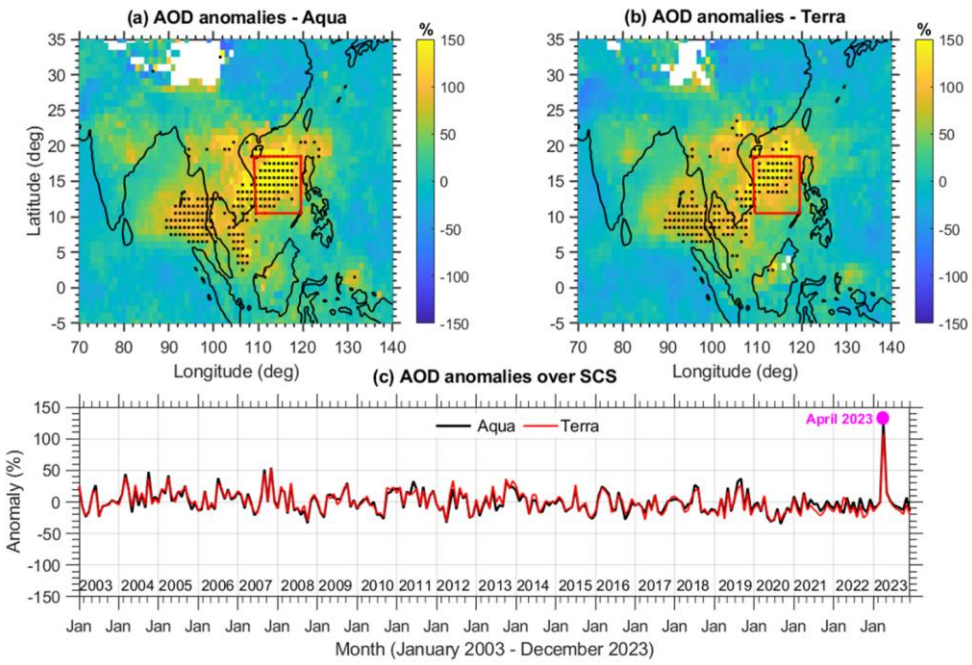

Figure 4. Spatial distribution of the change (%) in Aerosol Optical Depth (AOD) values during April 2023 compared with the inter-annual April average (2003-2022). (a) AOD anomalies are obtained from the MODIS Aqua and (b) from the MODIS Terra satellite. The black dots indicate that the anomalies exceed 4σ of the long-term mean. (c) Time series of area-averaged AOD anomalies expressed in percentage change over the South China Sea (SCS) domain from the Aqua (black line) and Terra (red line) satellites. The most pronounced enhancement occurred over the SCS, where April AOD anomalies exceeded 4σ above the long-term mean.

Figures 4a and **4b** depict the spatial extent of AOD anomalies expressed as percentage changes from MODIS Aqua and Terra. A surprising and widespread enhancement, with an increase of over 150% in most of the SCS and the southern Bay of Bengal (BoB), was evident in April 2023, and the increased anomalies exceeded approximately four standard deviation units. The area-averaged AOD anomalies (%) over the SCS domain from Aqua (black line) and Terra (red line) satellites show that the increase in April 2023 was a record high compared to MODIS data from 2003 to 2023, highlighting the extremity of AOD enhancement in that month. Satellite observations were further corroborated by ground-based in situ measurements from the AERONET. The only operational AERONET remote station downwind of PSEA biomass

burning, with over a decade of continuous AOD measurements (**Fig. S2a** in the Supplement), within the SCS region is located on Dongsha Island (also known as Pratas Island, 20.70°N, 116.73°E; 5 m a.s.l.). Analysis of the monthly mean AOD data from Dongsha Island indicates that April 2023 recorded the highest AOD value in the entire observational period from January 2009 to December 2023 (**Fig. S2c** in the Supplement). AERONET comparisons show strong correlations with MODIS AOD: 0.86 for Aqua and 0.87 for Terra (Sup. Fig. 3), supporting the reliability of the satellite observations. As AOD is a column-integrated measure, it does not provide information on the vertical distribution of aerosols. To overcome this limitation, we further analyzed vertical distribution images of aerosols from the Cloud-Aerosol Lidar and Infrared Pathfinder Satellite Observation (CALIPSO), which reveal pronounced enhancements in smoke aerosol over the SCS (**Fig. 5**). Elevated smoke layers were also observed over the southern BoB in April 2023, predominantly within the mid-troposphere at altitudes of approximately 2–5 km. Consistent with these lidar observations, MERRA-2 reanalysis data indicate substantial increases in aerosol mass concentrations in 2023, with black carbon (BC) increasing by ~250% and organic carbon (OC) by ~350% (**Fig. S4** in the Supplement). The most pronounced enhancements occur between 700 and 600 hPa, closely matching the altitude range identified by CALIPSO. The concurrence of satellite (MODIS and CALIPSO) and reanalysis data points to a severe pollution episode in April 2023 over and surrounding regions of the SCS, characterized by elevated aerosol layer indicative of long-range-transported biomass-burning smoke. Notably, the SCS is a relatively clean remote marine region with limited local aerosol sources. In such environments, enhanced aerosol loading is typically associated with long-range transport of pollutants from surrounding continental regions (Pani, 2023). Given the potential influence of long-range pollution transport, we further analyzed variations in carbon monoxide (CO), a widely used tracer of biomass-burning emissions due to its relatively long atmospheric lifetime (~1–2 months) and strong association with incomplete combustion (Ravindra Babu et al., 2023). We investigated CO changes across the study region using measurements from the MOPITT and AIRS satellites, which together provide more than two decades of continuous CO observations. CO data at 700 and 500 hPa from both satellites were analyzed for the period 2003–2023, with the 500 hPa level representing the altitude of maximum sensitivity for CO retrievals (Buchholz et al., 2021).

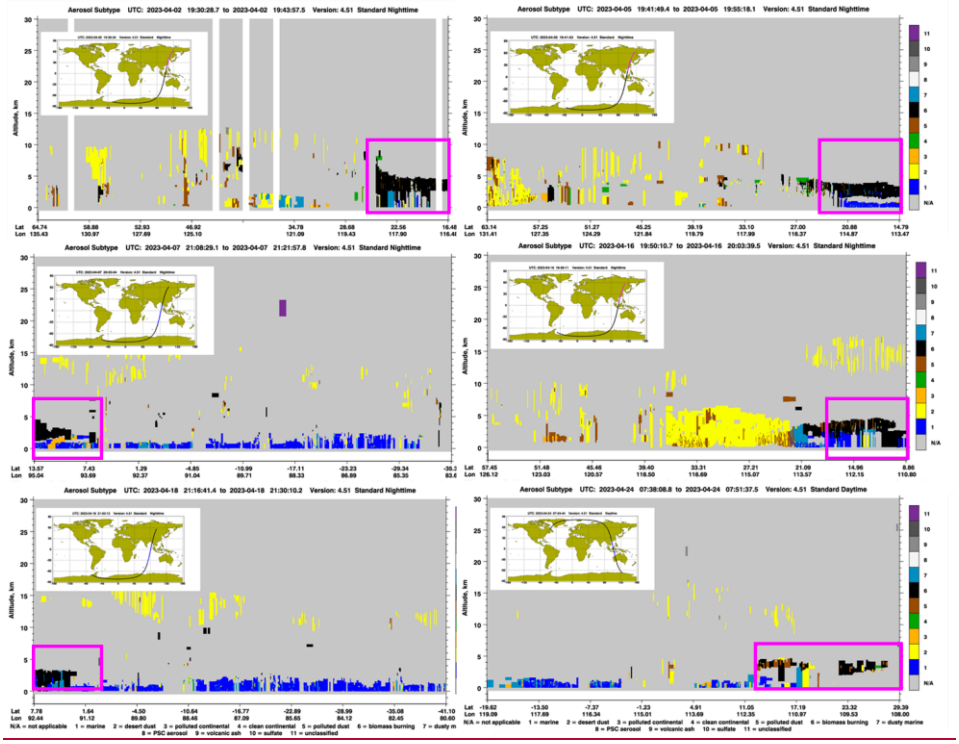

Figure 5. Aerosol subtype images obtained by the CALIPSO observations during various days in April 2023. The highlighted magenta box indicates elevated smoke over the SCS and the southern Bay of Bengal. Smoke aerosol is shown in black.

The observed CO anomalies from the two satellites are shown in **Fig. 6**, revealing significantly elevated CO concentrations over the SCS in April 2023, reaching up to 3σ above the 2003–2022 climatology. Although MOPITT displays more spatially concentrated anomalies than AIRS, both datasets consistently show positive CO anomalies at both pressure levels, indicating a substantial increase in mid-tropospheric CO during this period. For MOPITT CO retrievals, primary sources of uncertainty include limitations in vertical sensitivity and potential retrieval biases (Sayer et al., 2014; Wei et al., 2019). However, the observed enhancements (>3σ) are supported by independent AIRS CO measurements, reinforcing the robustness of the detected anomalies. The comparison between MOPITT and AIRS CO at 500 hPa over the SCS further shows a strong positive correlation (R ≈ 0.89; **Fig. S1b** in the Supplement). Furthermore, the

Formatted: Indent: First line: 0.5", Line spacing: 1.5 lines

spatial distribution of CO anomalies closely resembles that of AOD anomalies (Fig. 4). Area-averaged anomalies of AOD and 500 hPa CO over the SCS during 2003–2023 exhibit a strong positive correlation ($R \approx 0.81$; **Fig. S5** in the Supplement), suggesting that long-range pollution transport plays an important role in modulating April aerosol variability in this region. The bubble chart further highlights the exceptional severity of the April 2023 event compared with previous years (**Fig. S5** in the Supplement). Because CO is primarily produced through incomplete combustion, elevated concentrations far from major traffic or industrial sources strongly suggest biomass-burning and wildfire emissions. This indicates that smoke was likely transported from surrounding regions toward the SCS and the BoB, which are located near major biomass-burning hotspots, including the MC and PSEA. The MC fire season typically occurs from August to October, whereas PSEA experiences a biomass-burning season from January to April, peaking in March (**Fig. 2**). These seasonal characteristics strongly suggest that the elevated AOD levels observed over the SCS in April 2023 were likely linked to biomass-burning activity in PSEA. Overall, the April 2023 event is notable for its exceptional intensity and extensive spatial coverage. The MODIS AOD anomalies were approximately four times higher than the long-term mean across much of the SCS and the southern BoB during April 2023. We suggest that this episode represents a rare, previously unreported extreme aerosol-loading event, distinct from the springtime biomass-burning transport events over the PSEA region documented in earlier studies. Such anomalously high aerosol loading over the SCS may have important implications for regional air quality and climate, highlighting the need for further investigation into the underlying drivers and physical mechanisms responsible for this event.

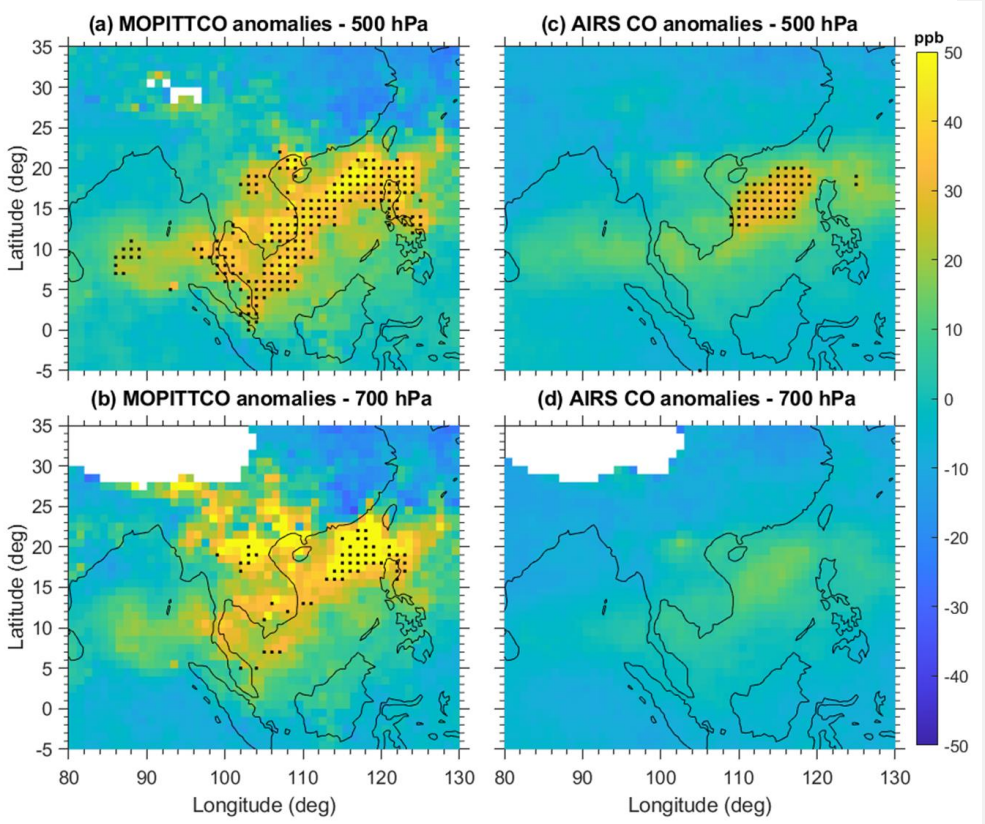

Figure 6. Spatial distribution of carbon monoxide (CO) anomalies in April 2023 at (a) 500 hPa and (b) 700 hPa from MOPITT satellite measurements. Panels (c) and (d) show the corresponding CO anomalies at 500 hPa and 700 hPa derived from AIRS satellite observations. Anomalies are calculated relative to the long-term April mean for 2003–2022. Black dots indicate regions where anomalies exceed the 3σ significance threshold.

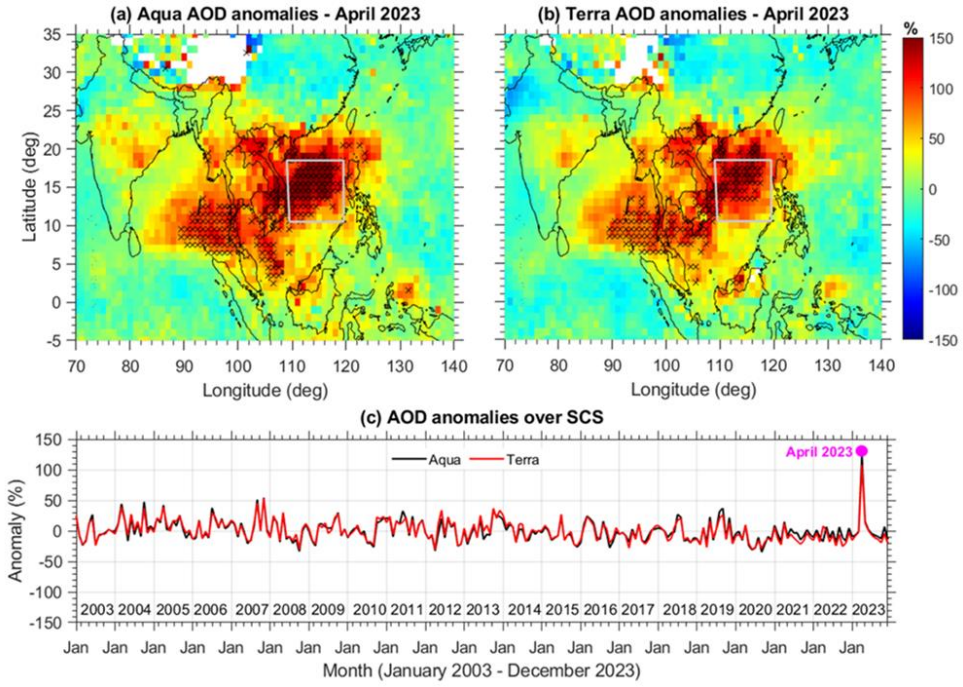

~~Figure 2.~~ ~~Spatial distribution of the change (%) in April 2023 Aerosol Optical Depth (AOD) values compared with the inter-annual April average (2003-2022). (a) AOD anomalies are obtained from the MODIS-Aqua and (b) from the MODIS-Terra satellite. The black hatches indicate that the anomalies exceed 4σ standard deviations of the long-term mean. (c) Time series of area-averaged AOD anomalies expressed in percentage change over the South China Sea (SCS) domain from the Aqua (black line) and Terra (red line) satellites. The most significant enhancement was in SCS, where the April AOD anomalies fell more than 4σ standard deviations.~~

~~The AOD distribution in April over two decades indicates high aerosol loading from northern Laos to coastal South China (15-25 N, 100-120 E). In April 2023, extreme AOD values extended from PSEA to South China and SCS, with the highest center between northern Laos and the SCS. Record-breaking AOD levels were observed for the area-averaged over the SCS in April 2023, showing a nominal increase in northern PSEA (**Sup. Fig. 2c-d**). The highest AOD value for northern PSEA in April 2023 correlates with record AOD over the SCS. To assess the magnitude of the increase, we estimated the percentage change in AOD by comparing April 2023 with the long-term average for April from 2003 to 2022. **Figures 2a** and **2b** depict the spatial extent of AOD anomalies expressed as percentage changes from MODIS-Aqua and Terra. A surprising and~~

widespread enhancement, with an increase of over 150% in most of the SCS and the southern Bay of Bengal (BoB), was evident in April 2023, and the increased anomalies exceeded approximately four standard deviation units. The area-averaged AOD anomalies (%) over the SCS domain from Aqua (black line) and Terra (red line) satellites show that the increase in April 2023 was a record high compared to MODIS data from 2003 to 2023, highlighting the extremity of AOD enhancement in that month. Satellite observations were further corroborated by ground-based in situ measurements from the AErosol RObotic NETwork (AERONET). The only operational AERONET remote station downwind of PSEA biomass burning, with over a decade of continuous AOD measurements (**Sup. Fig. 3a**), within the SCS region is located on Dongsha Island (also known as Pratas Island, 20.70°N, 116.73°E; 5 m a.s.l.). Analysis of the monthly mean AOD data from Dongsha Island indicates that April 2023 recorded the highest AOD value in the entire observational period from January 2009 to December 2023 (**Sup. Fig. 3c**).

We further investigated CO changes in April 2023 across the study region using MOPITT and AIRS satellite measurements, which provide over two decades of continuous CO data. CO is a crucial trace gas due to its role as a tropospheric pollutant, atmospheric transport tracer, and involvement in tropospheric chemistry. We analyzed CO data at 700 and 500 hPa from both satellites between 2003 and 2023. The 500 hPa level is the most sensitive altitude for CO measurements (Buchholz et al., 2021). The observed CO anomalies from the two satellites are shown in **Figure 3**, highlighting significantly elevated CO levels in April 2023 over the SCS, with increases up to 3σ standard deviations compared to the climatology from 2003 to 2022. Both instruments reveal distinct spatial anomalies, with MOPITT displaying more concentrated CO anomalies than AIRS. However, both show positive CO anomalies at both levels, indicating a significant increase in CO in April 2023. It is worth noting that the spatial distribution of CO anomalies aligns closely with AOD anomalies (**Fig. 2**). The area-averaged anomalies of AOD and 500 hPa CO over the SCS from 2003 to 2023 revealed a significant positive correlation of approximately 0.65 (**Sup. Figure 4**). This strong correlation in April (2003–2023) suggests that long-range pollution transport likely drives AOD variability in this region during April. The bubble chart illustrates the severity of April 2023 compared to other years over the SCS (**Sup. Figure 4**). CO production from incomplete combustion indicates that elevated levels far from traffic or industrial sources suggest biomass burning and wildfire emissions. This implies smoke transport from surrounding regions to the SCS and the BoB, near significant BB hotspots, including the MC

~~and PSEA. **Sup. Figure 1c-1d** shows annual AOD fluctuations, with peaks in April over PSEA and September over MC. The MC's fire season is from August to October, while PSEA experiences a BB season from January to April, peaking in March. This strongly suggested that the high AOD levels in April 2023 over the SCS were linked to BB activities in PSEA.~~

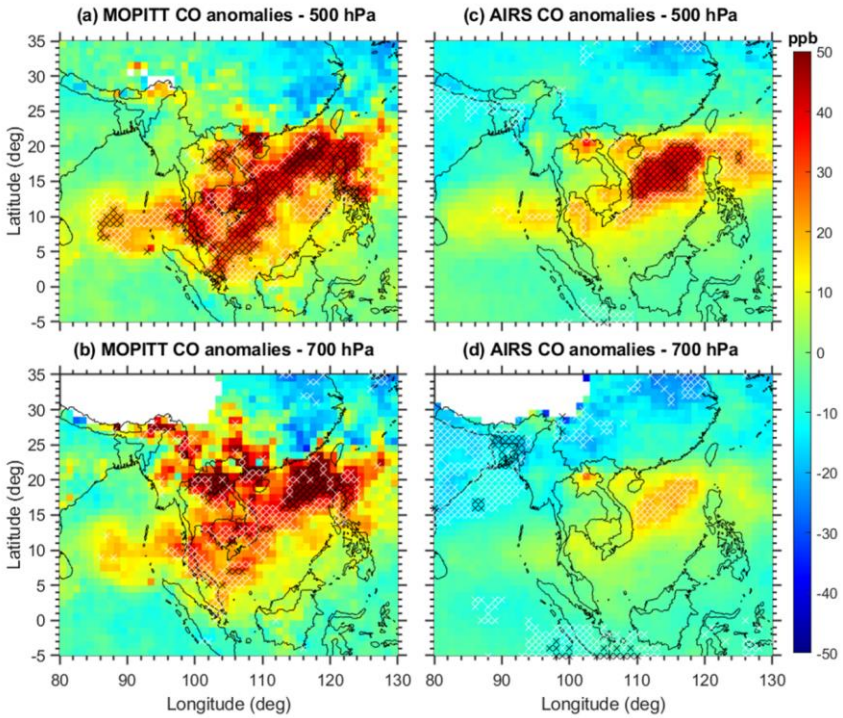

~~**Figure 3.** Spatial distribution of carbon monoxide anomalies in April 2023 at (a) 500 hPa and (b) 700 hPa obtained from MOPITT satellite measurements. Subplots (c) and (d) are identical to subplots (a) and (b), but the results are obtained from AIRS satellite measurements. The anomalies compared to the long-term mean of April from 2003 to 2022. The black and white hatches indicate that the anomalies are more significant than 3σ and 2σ standard deviations, respectively.~~

3.2 Transport and Source Attribution of the April 2023 Aerosol Event~~Biomass Burning activity over PSEA in April 2023~~

From the previous section, it is clear that most of the aerosols are free-troposphere-dominated and are located mostly in the ~2-5km region over SCS. To determine the source regions responsible for elevated aerosol concentrations over the SCS in April 2023, backward air-mass trajectories were computed using the HYSPLIT model. Trajectories were initialized at 15°N, 115°E, at 3 km above sea level, corresponding to the altitude range (2–5 km) of the elevated aerosol layer observed in CALIPSO and MERRA-2 profiles. Daily 72-hour trajectories (**Fig. 7a**) indicate that air masses arriving over the SCS predominantly originated from northern PSEA. When overlaid on the monthly mean MODIS AOD (**Fig. 7b**), these trajectories reveal transport pathways that coincide with regions of high aerosol loading, confirming that long-range transport from northern PSEA was the primary mechanism delivering BB emissions to the SCS. To see the BB activity in April 2023, we used MODIS fire counts and Burned Area. The spatial distributions of MODIS fire counts and burned area (BA) for April 2023 (**Figs. 8a–b**) show that BB activity was overwhelmingly concentrated in northern PSEA, particularly in northern Laos and adjacent regions of Myanmar and Thailand. Minimal fire activity and BA were observed over the MC and southern China; these regions were therefore excluded from source-region calculations. Analysis of inter-annual variability in April BB activity over PSEA from 2003 to 2023 (**Figs. 8c–d**), considering only fire detections above the 80% confidence level, indicates substantial year-to-year fluctuations. Notably, April 2023 recorded the highest burned area (~2.27 Mha) during the 21-year period, highlighting the exceptional intensity of BB activity during this month.

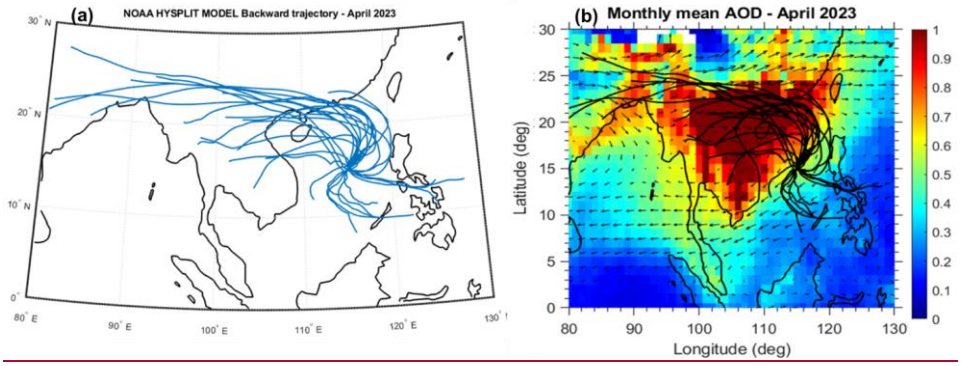

Figure 7. (a) Daily 72-h NOAA HYSPLIT backward trajectories ending at 12:00 UTC at a representative location (15°N, 115°E) over the South China Sea at 3 km altitude for April 2023.

Formatted: Font: Bold, Font color: Auto

Formatted: Font color: Auto

(b) Same as (a), but overlaid on the monthly mean MODIS aerosol optical depth (AOD) for April 2023.

Formatted: Indent: First line: 0"

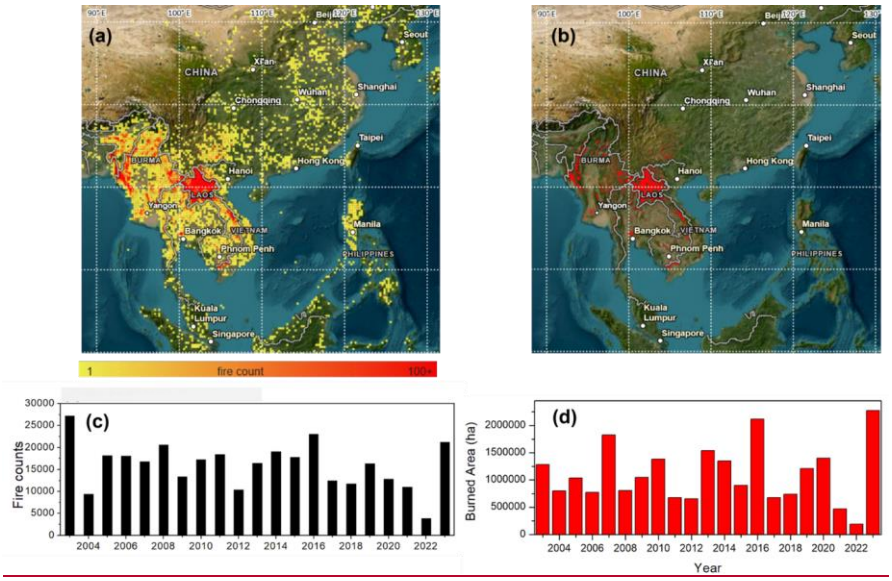

Figure 8. Spatial distribution of the (a) MODIS fire counts, (b) MODIS Global Burned Area Product in April 2023. Inter-annual variability in (c) Fire counts, and (d) Burned Area over Peninsula Southeast Asia in April from 2003 to 2023. (Source: https://firms.modaps.eosdis.nasa.gov/). For inter-annual variability in fire counts, we considered those above the 80% confidence level.

Country-level statistics (**Table 2**) further highlight the dominant contribution from Laos, which accounted for 11,877 fires (56.0%), 1.53 × 10^6 MW of fire radiative power (FRP; 63.5%), and 1.08 × 10^6 ha of burned area (47.7%). Notably, the BA observed in April 2023 represents the highest monthly value in the available dataset (2002–2023; **Fig. S6** in the Supplement). Approximately 60% of Laos is forested (**Fig. S7** in the Supplement), with much of this forest located in northern Laos where the majority of fires occurred during April 2023 (**Fig. 8a**). Myanmar contributed the second-largest share, with 7,054 fires (33.3%), 7.78 × 10^5 MW of FRP (32.3%), and 9.15 × 10^5 ha of burned area (40.3%). Thailand, Vietnam, and Cambodia contributed comparatively smaller burned areas of 1.21 × 10^5 ha, 1.30 × 10^5 ha, and 2.20 × 10^4 ha, respectively. In total, 21,198 fires across PSEA produced approximately 2.41 × 10^6 MW of FRP in April 2023.

These results indicate that intense BB activity over northern PSEA, particularly northern Laos, was the primary source of the exceptional aerosol loading observed over the SCS in April 2023. However, two key questions remain: (i) what factors triggered the anomalously strong fire activity in Laos during April 2023, and (ii) why were BB aerosols transported unusually far southward across the SCS and into the southern BoB, rather than following the more typical transport pathways toward Taiwan and the north western Pacific? To address these questions, we next examine the large-scale meteorological and dynamical circulation conditions prevailing during April 2023.

Table 2. MODIS total fire counts, the corresponding total accumulated fire radiative power (FRP), and the burned area (BA) observed over peninsular Southeast Asia (PSEA) and each country within PSEA in April 2023. The percentage contribution of each country to the total number of fires, the total FRP, and the BA of PSEA is shown in brackets.

Country	**Total Fires**	**Fire Radiative Power (MW)**	**Burned Area (ha)**
PSEA	21198	2407283	2272099.89
Country	Total Fires	FRP	BA
Cambodia	242 (1.14%)	13402 (0.5%)	21959.5 (0.97%)
Laos	11877 (56.02%)	1530000 (63.5%)	1084050 (47.71%)
Myanmar	7054 (33.27%)	777970 (32.32%)	915175.7 (40.27%)
Thailand	1322 (6.24%)	50276 (2.1%)	120573.7 (5.31%)
Vietnam	703 (3.32%)	35634 (1.5%)	130340.7 (5.74%)

Formatted: Indent: First line: 0"

3.3 Large-scale meteorological and dynamical circulation anomalies in April 2023

Formatted: Indent: First line: 0.5"

In this section, we examine the meteorological and large-scale dynamical circulation anomalies associated with the April 2023 event. **Figure 9** presents the spatial distribution of anomalies in key meteorological parameters during April 2023 relative to the 2003–2022 climatological mean. As shown in **Figure 9**, anomalies in Outgoing Longwave Radiation (OLR) indicate suppressed convective activity over PSEA during April 2023. The reduced convection

was accompanied by negative precipitation anomalies, elevated surface temperatures, and pronounced soil moisture (SM) deficits. These conditions are spatially consistent with the regions of enhanced fire counts and burned area observed by MODIS over northern Laos (**Fig. 8**). Long-term SM anomalies over northern Laos reached exceptionally low values in April 2023, representing the lowest levels in the past two decades (**Figs. S8a–b** in the Supplement). To further examine the persistence of these conditions, we analyzed the temporal evolution of SM anomalies during 2021–2023. The results show maximum positive anomalies in March 2022 and a transition to strong negative anomalies by April 2023, indicating a prolonged drought from winter 2022 to April 2023 (**Fig. S8c** in the Supplement). We further assessed the relationship between SM anomalies and fire activity over Laos. The standardized fire anomalies and SM anomalies (**Fig. S9** in the Supplement) reveal a significant inverse relationship: reduced SM is associated with enhanced fire activity. In April 2023, extreme negative SM anomalies coincided with strong positive fire anomalies, highlighting the role of severe surface drying in promoting intense biomass-burning activity. A similar co-occurrence of anomalously low SM and elevated fire activity is also evident in 2016, a year previously identified as having intensified regional burning. These findings provide additional observational evidence that soil moisture deficits are linked to enhanced fire activity over PSEA. Previous studies have shown that negative SM anomalies can promote positive geopotential height anomalies in the upper troposphere, which tend to reinforce local high-pressure conditions and enhance surface warming (e.g., Fischer et al., 2007; Dong et al., 2023). Motivated by this mechanism, we next examine the large-scale dynamical circulation patterns during April 2023 to understand how atmospheric dynamics may have contributed to the observed meteorological anomalies and the anomalous transport of biomass-burning aerosols.

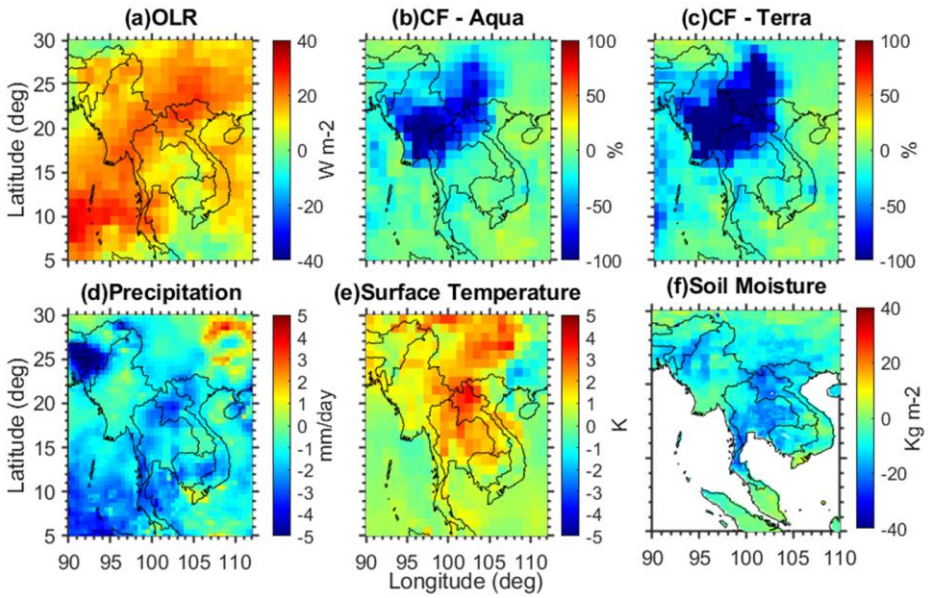

Figure 9. Surface and atmosphere conditions in April 2023. April anomalies in 2023 compared to the 2003-2022 climatological period for (a) Outgoing Longwave radiation (OLR), (b) cloud fraction (CF) from Aqua, (c) cloud fraction from Terra, (d) precipitation, (e) Surface Temperature, (f) soil moisture (10 - 40 cm underground). OLR and surface temperatures are obtained from AIRS satellite measurements. CF data from MODIS Aqua and Terra. Soil moisture is obtained from the GLDAS Noah Land Surface Model L4 monthly 0.25 x 0.25 degree V2.1. Precipitation data is obtained from the Global Precipitation Climatology Project (GPCP) Version 3.2.

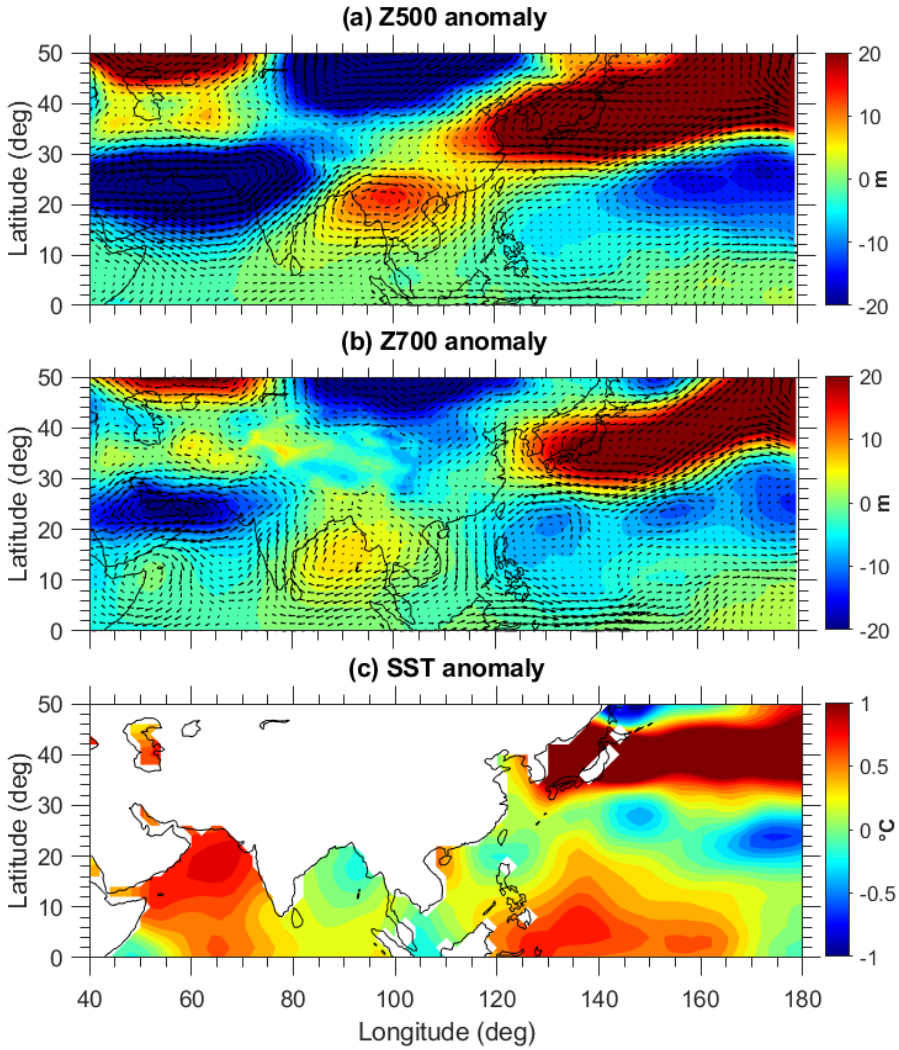

Figure 10. Spatial distribution of (a) 500 hPa geopotential height (Z500), (b) 700 hPa geopotential height (Z700), and (c) Sea Surface Temperature (SST) anomalies in April 2023. The anomalies are calculated by subtracting the April 2023 monthly mean from the April climatology for the period 1991 to 2020. The wind anomalies for the respective pressure levels are overlaid in Z500 and Z700 anomalies. The geopotential height and wind data are from the MERRA-2 reanalysis, while SST data are from the NOAA Extended Reconstructed SST V5.

Our analysis focuses on geopotential height and horizontal wind fields at the 700- and 500-hPa levels. The geopotential height fields (Z700 and Z500) in April 2023 show clear departures from the April climatology (1991–2020) (**Figs. S10–11** in the Supplement). At 700 hPa, the climatological high-pressure system over the Indian region extended eastward toward PSEA, while at 500 hPa the western Pacific subtropical anticyclone shifted westward to lie directly over PSEA. Geopotential height anomalies relative to the 1991–2020 mean (**Fig. 10a–b**) reveal a pronounced anti-cyclonic circulation centered over northern PSEA (~20°N, 100°E). Cyclonic anomalies over the WNP near the Philippines and upstream over the Indian Ocean form a zonal low–high–low (L–H–L) structure, consistent with a propagating Rossby wave train (Hu et al., 2024). An additional anti-cyclonic anomaly is present over the mid-latitude North Pacific. These circulation anomalies suppressed convection over PSEA, consistent with positive OLR anomalies and reduced precipitation (**Fig. 9**). Subsidence associated with the anti-cyclonic circulation promoted clear-sky conditions (**Fig. 9**) and surface warming, which, together with severe soil moisture deficits, created favorable conditions for intense biomass burning across northern Laos. The circulation pattern also altered regional transport pathways. The combined influence of the WNP cyclone, the BoB anticyclone at 700 hPa, and the PSEA anticyclone at 500 hPa modified the background flow over Southeast Asia. Meridional wind anomalies (**Figs. S12b–c** in the Supplement) show persistent northerly flow over the SCS, enabling southward transport of smoke from northern PSEA toward the SCS and further into the southern BoB. This pathway contrasts with the climatological transport route that typically advects smoke toward Taiwan and the northwestern Pacific. Zonal wind anomalies further indicate weakened mid-latitude westerlies and locally reversed easterlies near Japan associated with a strong anti-cyclonic anomaly (**Figs. S12a–b** in the Supplement), suppressing the typical eastward export of smoke. Consistent with this, AOD observations from the high-altitude mountain Lulin Atmospheric Background Station obtained through AERONET show no notable enhancement in April 2023 (**Fig. S13a** in the Supplement), indicating reduced smoke transport toward the northwestern Pacific. AERONET comparisons show strong correlations with MODIS AOD: 0.83 for Aqua and 0.84 for Terra (**Fig. S14** in the Supplement), further supporting the reliability of the satellite observations as shown in the Dongsha data. Overall, the anomalous circulation pattern, characterized by a BoB anticyclone and a WNP

Formatted: Indent: First line: 0.5"

cyclone, redirected biomass-burning plumes from northern PSEA toward the SCS and southern BoB, producing the exceptional aerosol loading observed in April 2023.

A key question is whether 2023 represents an exceptional biomass-burning (BB) year relative to PSEA, or if similar conditions have occurred in other high-BB years. High-BB years were identified using standardized fire anomalies from MODIS fire counts, with years exceeding 0.5 classified as high-BB (**Fig. S9** in the Supplement). Composites of MODIS AOD, 500-hPa geopotential height, and wind vectors were constructed to represent typical circulation and aerosol patterns during high-BB periods. Comparison with April 2023 shows notable differences: 2023 featured a stronger, more spatially coherent anti-cyclonic high over PSEA and substantially higher AOD, indicating unusually intense aerosol loading. This suggests that circulation anomalies in 2023 amplified aerosol accumulation and transport beyond typical high-BB conditions (**Fig. S15** in the Supplement). Another question is whether inter-annual variability associated with climate oscillations, such as the El Niño–Southern Oscillation (ENSO), influenced BB activity and circulation in 2023. SST anomalies linked to ENSO strongly modulate Indo-Pacific circulation and hydro climate, with El Niño events typically enhancing springtime fires via drought, reduced precipitation, and suppressed moisture transport (Yin, 2020; Zhu et al., 2021; Zheng et al., 2023). We constructed composites of MODIS AOD and 500-hPa wind vectors for El Niño–ensuing and La Niña–ensuing Aprils during 2003–2022 (**Fig. S16** in the Supplement). The results reveal higher AOD over northern PSEA and coastal South China during El Niño-ensuing Aprils, accompanied by a stronger anti-cyclonic system over PSEA extending from the BoB, consistent with enhanced aerosol accumulation. In contrast, La Niña-ensuing Aprils show weaker circulation and lower AOD. April 2023 occurred during the transition from a triple-dip La Niña to a developing El Niño, deviating from typical ENSO-fire patterns. The anomalous anti-cyclonic and cyclonic circulations over the BoB and western North Pacific in April 2023 are notable (**Fig. 10**), though their detailed dynamics are beyond the scope of this study. Preliminary analysis revealed that SST warming over the western Pacific warm pool and mid-latitude North Pacific, together with cooling over the central-eastern equatorial Pacific, likely induced a Matsuno-Gill-type response, while warming in the Arabian Sea and cooling in the BoB aligned with geopotential height anomalies, promoting drought, intensified BB, and southward smoke transport toward the SCS and southern BoB (**Fig. 10c**; Gill, 1980; Zeng and Sun, 2022). Overall, the extreme aerosol event in April 2023 was shaped not only by intense biomass burning but also by anomalous large-scale circulation linked to ocean–

atmosphere variability, highlighting the combined role of local and climate-scale drivers in exceptional smoke events.~~We further examined BB activity over PSEA in April 2023, using MODIS fire counts and fire radiative power (FRP) as proxies for BB activities and wildfires. It is noted that there were a total of 21198 fire counts and a total FRP of 2407283 (MW) throughout PSEA (**Sup. Table 1**). Fire counts and FRP varied significantly between countries, with Laos reporting the highest number of fire counts (11877) and FRP (1530000 MW). Notably, Laos accounted for 56% of the total fire counts and 63% of the FRP for PSEA, establishing it as a hotspot for BB activity in April 2023. **Figures 4a** and **b** show the spatial distribution of fire counts and the related FRP over PSEA in April 2023. Persistent and more intense fires were observed over northern Laos and Myanmar, with the most intense fires occurring north of Laos. The number of fires in Laos in April 2023 was the highest recorded in the past 20 years (**Fig. 4c**). It should be noted that Laos is characterized by around 60% of its land cover types being forests (**Sup. Fig. 5**). Most of this forest is situated in northern Laos, where most fires occurred in April 2023. This suggests that forest fires in Laos were primarily responsible for the majority of fires in 2023. Although the FRP in 2023 was not at its peak, it was still among the highest BB activities, following 2016 and 2003. However, the nighttime fires and corresponding FRP demonstrate that the 2023 BB activity was the highest in the entire MODIS data record and exceptionally intense in terms of FRP (**Figs. 4e-4f**). This demonstrated the intensity of the fires in April 2023 compared to the last 20 years. The extreme nighttime fire activity highlights changes in fire behavior and environmental or human factors that favored intense nighttime burning in April 2023. We further examined area-averaged fires and FRP over northern Laos (17-23°N), indicating that the highest fires and FRP were recorded in April 2023 in MODIS data from January 2003 to December 2023 (**Sup. Fig. 6**). Furthermore, the MODIS estimated monthly burned area product (MCD64A1) reveals a total area of 1.08 million hectares burned in Laos in April 2023, the highest monthly value in the available data for that dataset (2002–2023; **Sup. Fig. 7**). The spatial distribution of the MODIS burned area (**Sup. Fig. 8a**) shows that the most significant area affected by fires in 2023 was located in northern Laos, which closely aligns with the total number of fires and the FRP illustrated in **Figure 4**. This raises the question: What caused the anomalous fire activity in Laos in April 2023? We examined various meteorological and dynamic conditions in April 2023 to address this.~~

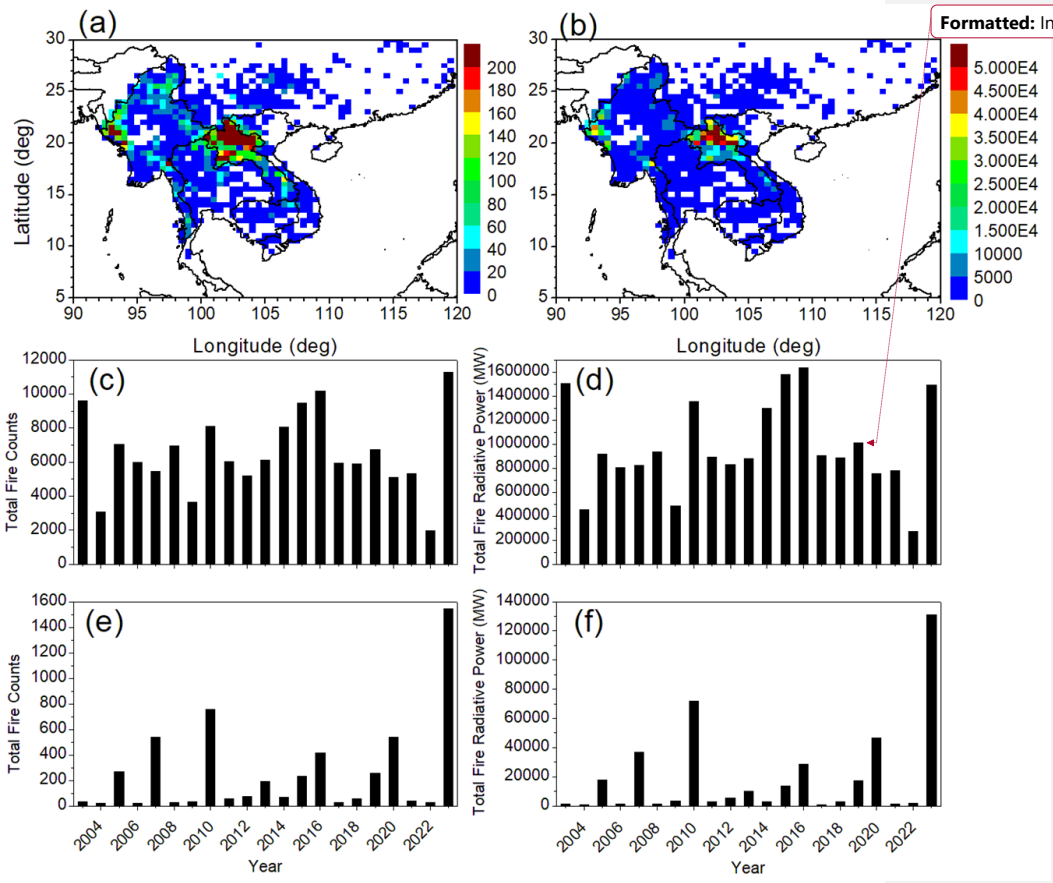

Formatted: Indent: First line: 0.5"

Figure 4. Spatial distribution (0.25° × 0.25°) of MODIS (a) fire counts and (b) total fire radiative power (FRP) in April 2023. A notable increase in fire activity over northern Laos is observed. (c) Inter-annual (2003 to 2023) monthly fire counts (day and night), and (d) the total FRP for April over Laos. (e) Inter-annual monthly nighttime fire counts and (f) the total FRP for nighttime fire counts over Laos in April. Fires with a confidence level of more than 80% are considered for the present analysis.

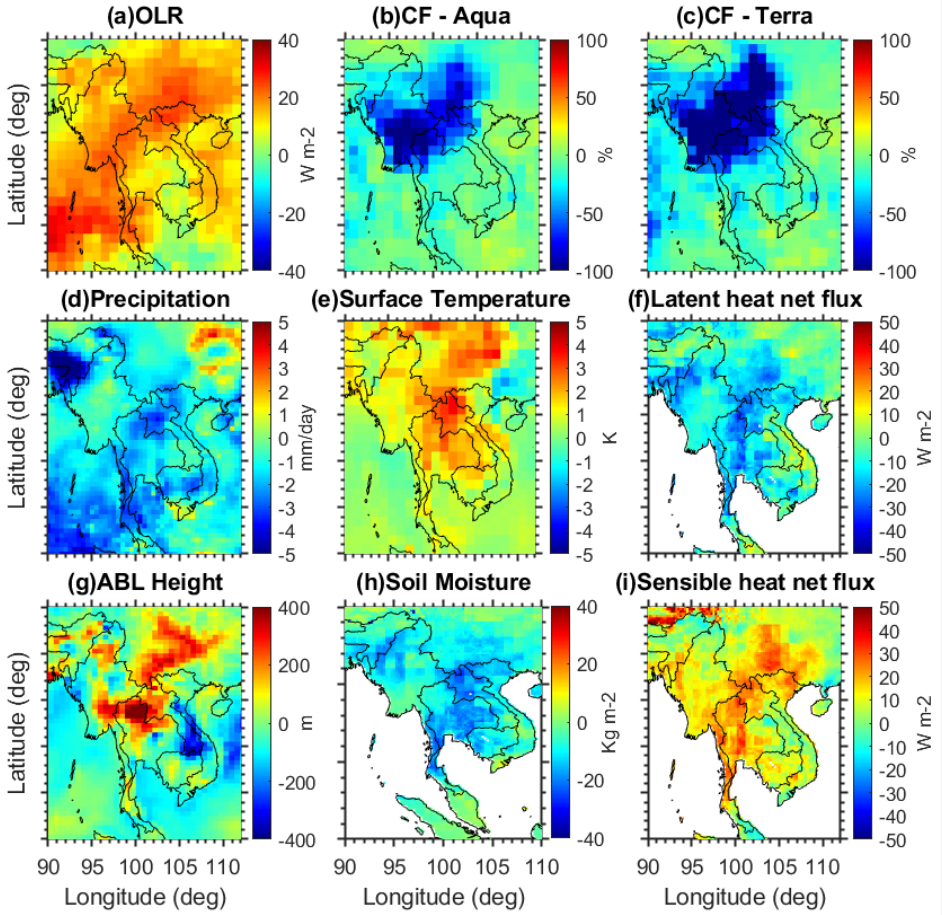

694

695 **~~Figure 5~~**. ~~Surface and atmosphere conditions in April 2023. April anomalies in 2023 compared to~~
696 ~~the 2003-2022 climatological period for (a) Outgoing Longwave radiation (OLR), (b) cloud~~
697 ~~fraction (CF) from Aqua, (c) cloud fraction from Terra, (d) precipitation, (e) Surface Temperature,~~
698 ~~(f) surface latent heat flux, (g) Atmospheric Boundary Layer (ABL) Height, (h) soil moisture (10~~
699 ~~– 40 cm underground), and (i) surface sensible heat flux. OLR and surface temperatures are~~
700 ~~obtained from AIRS satellite measurements. CF data from MODIS Aqua and Terra. ABL height~~
701 ~~obtained from MERRA-2 reanalysis. Soil moisture, surface latent heat, and sensible heat flux are~~
702 ~~obtained from the GLDAS Noah Land Surface Model L4 monthly 0.25 x 0.25 degree V2.1.~~
703 ~~Precipitation data is obtained from the Global Precipitation Climatology Project (GPCP) Version~~
704 ~~3.2.~~

705 ~~In April 2023, Outgoing Longwave Radiation (OLR) anomalies reflected decreased~~
706 ~~convective activity over PSEA, resulting in reduced precipitation, higher temperatures, and low~~

soil moisture (SM), as shown in **Fig. 5**. Precipitation, temperature, and SM anomalies correlate with enhanced MODIS fire counts and FRP over northern Laos (**Fig. 4**). Long-term SM anomalies in northern Laos reached record lows in April 2023, the lowest in two decades (**Sup. Figs. 9a and b**). We further examined the evolution of SM anomalies during 2021-2023, which indicates maximum positive values in March 2022 and maximum negative anomalies in April 2023, signifying prolonged drought from winter 2022 to April 2023 (**Sup. Fig. 9c**). Interestingly, the record-low SM anomalies occurred during the transition period from La Niña to El Niño. Under dry conditions, increased sensible heat flux warms the near-surface atmosphere, resulting in a positive land-atmosphere feedback (Alexander 2011). To explore how record SM anomalies in April 2023 affected land-atmospheric coupling, we analyzed surface heat flux changes over PSEA, revealing decreased surface latent heat flux and increased sensible heat flux. The negative latent heat flux anomalies indicated limited evapotranspiration due to dry soil conditions. A deeper Atmospheric Boundary Layer (ABL) height (>400 m increase) was observed over northern PSEA, particularly in Laos, aligning with other anomalies in April 2023. Negative SM anomalies favor a positive geopotential height anomaly in upper levels, maintaining local high pressure and promoting surface warming (Fischer et al., 2007; Dong et al., 2023). The northern PSEA experienced a high-pressure anticyclone in April 2023 (**Fig. 6a**), which decreased cloud cover, increased solar radiation and surface temperature, and reduced precipitation. MODIS cloud fraction (CF) anomalies exhibited extreme negative values, particularly in the northern PSEA, decreasing by over 100% compared to the 2003-2022 average, closely aligning with the high-pressure anticyclone depicted in **Figure 6a**. Reduced cloud cover and drier soil will increase heat, landscape flammability, and wildfire potential. It is concluded that record-breaking negative SM anomalies under a deeper, drier, and warmer ABL, coupled with increased temperatures, low precipitation, and anomalous low cloud cover associated with the upper tropospheric high-pressure system, contributed to record-breaking BB and wildfires over Laos in April 2023.

3.3 Dynamical and large scale circulations in April 2023

Previous research shows that in spring, smoke aerosols (BC and OC) and trace gases are transported from PSEA to downstream areas like southern SC, Taiwan, and the northwestern Pacific via free tropospheric westerlies (Wai et al., 2008; Lin et al., 2009; Lin et al., 2013; Yen et al., 2013; Chuang et al., 2014; Ou-Yang et al., 2014; Lin et al., 2017; Pani et al., 2019).

Remarkably, in April 2023, PSEA BB smoke aerosols and trace gases were transported to the far southern regions of the SCS and the BoB, marking a significant departure from the usual transport pathway to downwind Taiwan and the northwest Pacific, respectively.

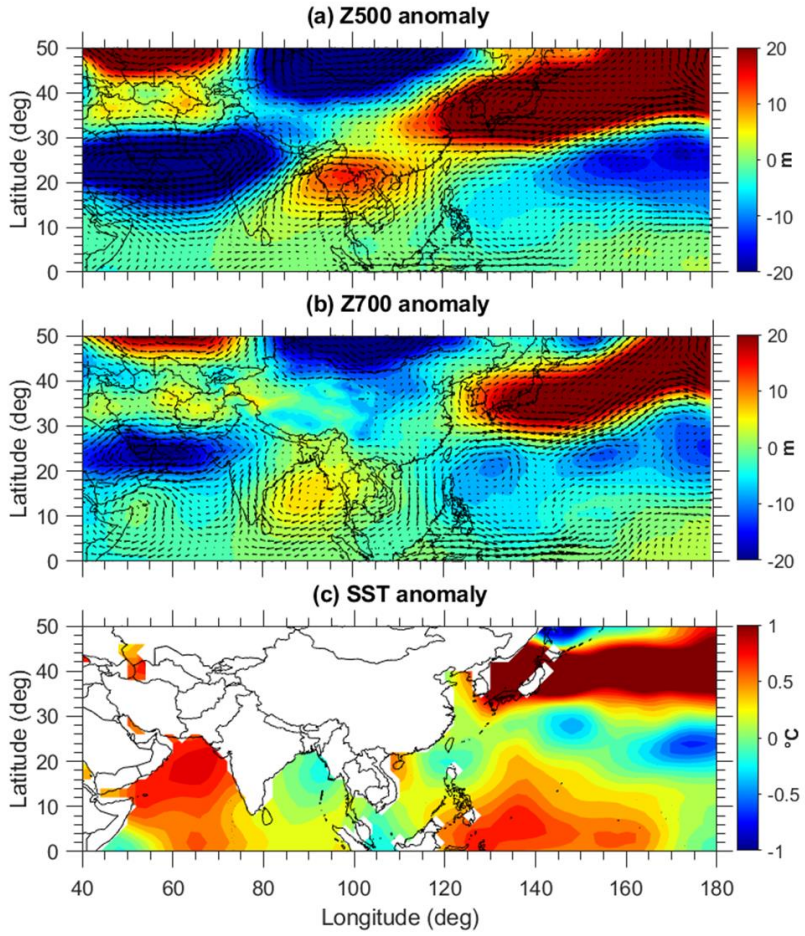

Figure 6. Spatial distribution of (a) 500 hPa geopotential height (Z500), (b) 700 hPa geopotential height (Z700), and (c) Sea Surface Temperature (SST) anomalies in April 2023. The anomalies are calculated by subtracting the monthly mean of April 2023 from the April climatology for the period from 1991 to 2020. The wind anomalies for the respective pressure levels are overlaid in Z500 and Z700 anomalies. The geopotential height and wind data are from the MERRA-2 reanalysis, while SST data are from the NOAA Extended Reconstructed SST V5.

~~Here, background dynamics and large-scale circulations are crucial for transporting smoke aerosols over longer distances from the sources (Ravindra Babu et al., 2023; Huang et al., 2024). To provide context for the April 2023 event, we briefly analyzed the large-scale circulation patterns responsible for the unprecedented aerosol loading. Our focus was on the geopotential height and winds, both zonal and meridional, at 700 and 500 hPa levels. The geopotential height observed at these levels (Z700 and Z500) in April 2023 contrasts with the background climatology of April (1991-2020) (**Sup. Figs. 10 and 11**). Specifically, at 700 hPa (Z700), a high pressure system over the Indian region shifted eastward, reaching the PSEA. In comparison, at 500 hPa (Z500), the western Pacific anticyclone shifted westward to sit directly above the PSEA. To get a clearer picture, we further obtained the anomaly in Z700 and Z500 in April 2023 by comparing the long-term mean of 1991-2020. The observed Z700 and Z500 anomaly composites are illustrated in **Figure 6a and b**. There is a prominent anomalous anticyclone over northern PSEA, centered roughly at 20°N, 100°E (**Fig. 6a**). Additionally, a significant anomalous low-level cyclone is present over the western North Pacific (WNP) around the Philippines, with an anomalous cyclone forming upstream and downstream of the anticyclone over the PSEA, creating a zonal low-high-low (L-H-L) pattern. This arrangement might suggest the movement of a Rossby wave train (Hu et al., 2024). Concurrently, a strong anticyclone anomaly was situated over the northern Pacific Ocean, just above the western Pacific cyclone anomaly. It is strongly indicated from **Figures 5** and **6** that the upper- and lower-level anomalous anticyclones significantly caused cloudless skies, reduced precipitation, and elevated surface temperatures in the PSEA. These favorable conditions, occurring over drier soil, led to extreme BB and wildfires in Laos, which released significant quantities of aerosols and trace gases into the atmosphere.~~

~~We hypothesize that these systems, including an anomalous WNP cyclone, a BoB anticyclone at 700 hPa, and a high-pressure anticyclone over PSEA at 500 hPa, substantially influenced the background circulations in the PSEA and its surroundings. This interaction likely contributed to the unusual BB smoke transport from northern PSEA to the SCS and the BoB in April 2023, as corroborated by the meridional wind anomalies in **Sup. Figs. 12b and c**, which indicate unusual northerly winds over the SCS. The northerly wind anomalies inhibited smoke transport from northern PSEA to the SCS, resulting in unprecedented aerosol loading over the SCS and the BoB. Additionally, zonal wind anomalies showed typical background westerlies supplanted by easterlies over the North Pacific near Japan, due to an anomalous high-pressure~~

system in April 2023 (**Sup. Figs. 12a and b**). This high-pressure system weakened the westerlies to its south, obstructing the usual smoke transport from PSEA to the downwind northwestern Pacific. This is further supported by AERONET observations from Lulin Atmospheric Background Station (LABS, 23°28′N, 120°52′E, 2,862 m; Sheu et al., 2010), located downwind of the PSEA smoke (**Sup. Fig. 12a**). The AOD data revealed no notable rise in AOD at Lulin in April 2023 compared to previous years, similar to what was observed at Dongsha Island (**Sup. Fig. 13c**). In conclusion, the unusual circulation from the BoB anticyclone and the WNP cyclone transported PSEA smoke into the SCS, resulting in unprecedented aerosol loading in April 2023. Exploring the causes and dynamics behind the anti-cyclonic and cyclonic circulations over the BoB and WNP in April 2023 is intriguing; however, it falls outside the scope of this study. Preliminary analysis of sea surface temperature (SST) anomalies in April 2023 revealed a distinct and spatially coherent pattern across the Pacific Ocean (**Fig. 6c**). Notably, positive SST anomalies were observed over the western Pacific warm pool near the equatorial region, while negative anomalies appeared over the central to eastern equatorial Pacific. In addition, strong positive SST anomalies were present over the mid-latitude North Pacific. This tri-polar SST structure is known to influence large-scale atmospheric circulation patterns. According to the Matsuno-Gill framework, enhanced warming in the tropical western Pacific can induce anomalous cyclonic circulation over the WNP (Gill, 1980; Zeng and Sun, 2022). Concurrently, regional SST anomalies over the Indian Ocean exhibited positive values in the Arabian Sea and negative anomalies in the BoB. These SST anomalies corresponded closely with 700-hPa geopotential height (Z700) anomalies, which were positive over the BoB and negative over the Arabian Sea. The spatial alignment of SST and Z700 anomalies suggests that the observed SST anomaly configuration in April 2023 likely exerted a substantial influence on tropospheric circulation over both the Indian and Pacific Oceans.

3.4 Impact on Tropospheric Ozone

It is well known that BB smoke can emit aerosols and various gaseous compounds, including nitrogen oxides (NO_x), CO, methane (CH_4), and multiple volatile organic compounds (VOCs). Once emitted, BB smoke undergoes chemical transformations in the atmosphere, altering the mix of compounds and generating secondary pollutants such as ozone (O_3) and secondary organic aerosol (Jaffe and Wigder, 2012; Ogino et al., 2022). BB emissions from the PSEA have a significant impact on air quality and weather in both source and downwind regions. In previous

sections, we demonstrated the record-breaking increase in AOD, along with the unusual enhancement in tropospheric CO (at 700 and 500 hPa) over SCS due to PSEA biomass burning. It is known that the presence of CO is one of the factors that control the abundance of tropospheric ozone, a short-lived pollutant and climate forcer (Liu et al., 1999; Chan et al., 2003; Ou-Yang et al., 2012; Yadav et al., 2017; Liao et al., 2021).

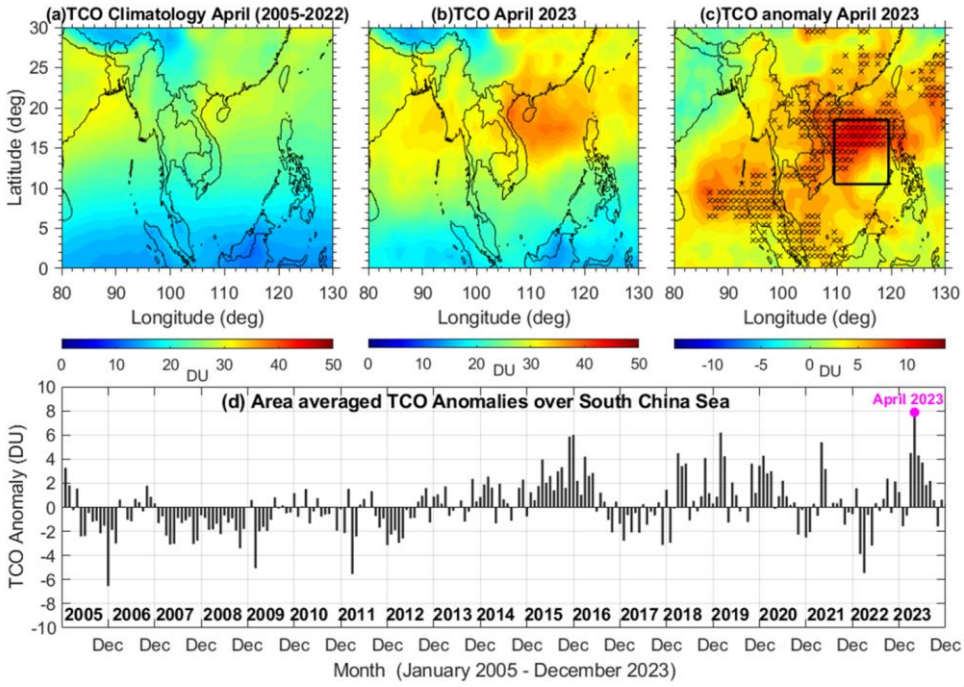

Figure 7. Spatial distribution of tropospheric column ozone (TCO) (surface – 300 hPa ozone column) concentrations in (a) April (2005-2022), (b) April 2023. (c). The observed spatial distribution of TCO anomaly in April 2023. Anomalies based on removing the 2005-2022 April mean. (d) The area-averaged TCO anomalies observed over SCS between January 2005 and December 2023 – anomalies based on removing the long-term mean from 2005 to 2022. The highest increase in the TCO for the SCS region is recorded in April 2023 during the OMI/MLS data period. The black hatches in sub-plot (c) indicate that the anomalies are more significant than 3σ standard deviations, respectively.

Here, we investigated how this record-breaking pollution event may have influenced tropospheric ozone levels in April 2023. We analyzed long-term tropospheric ozone column (TOC) data (surface to 300 hPa) from the combined Aura Ozone Monitoring Instrument and Microwave Limb

~~Sounder satellite ozone measurements (OMI/MLS) from 2005 to 2023 (Ziemke et al., 2006; 2019).~~ ~~**Figures 7a** and **7b** illustrate the spatial distribution of the long-term April mean and the April 2023~~ ~~TOC over the study area. Additionally, **Figure 7c** illustrates the observed anomaly in April 2023~~ ~~in comparison to the long-term average. We also include area-averaged TOC anomalies over the~~ ~~SCS spanning the entire OMI/MLS dataset. The OMI/MLS TOC anomaly indicates significantly~~ ~~elevated ozone levels over the SCS and nearby regions during April 2023. The observed anomalies~~ ~~are statistically significant, being three standard deviations above the long-term mean of total~~ ~~column ozone (TOC). Furthermore, the monthly mean anomalies, averaged over the SCS~~ ~~throughout the entire OMI/MLS data period, reveal the highest increase in TOC, approximately 8~~ ~~Dobson Units (DU), in April 2023. These exceptional TCO increases from the OMI/MLS data are~~ ~~further supported by the AIRS satellite O_3 measurements and the downwind ozonesonde~~ ~~measurements at Hong Kong, which are presented in **Sup. Figure 14**, respectively. We utilized~~ ~~long-term ozone measurements from the AIRS satellite from 2003 to 2023. Our analysis of 700~~ ~~and 500 hPa levels reveals a substantial O_3 increase over SCS and nearby areas, about 20 ppb,~~ ~~exceeding two standard deviations of the long-term mean, corroborated by downwind Hong Kong~~ ~~ozonesonde measurements **(Sup. Figs. 14c and d)**. The ozone profile peaks at altitudes of 3 to 4~~ ~~km, with anomalies exceeding 30 ppb in the 3 to 5 km region, correlating exactly with the~~ ~~CALIPSO vertical aerosol enhancement. This illustrates the exceptional augmentation of TOC~~ ~~over the SCS in April 2023, comparable to the AOD increase observed in the MODIS data. Such~~ ~~findings are corroborated by the corresponding increases in CO levels recorded by MOPITT and~~ ~~AIRS at 700 hPa and 500 hPa, respectively, indicating a substantial influence of BB plumes~~ ~~originating from the PSEA region in 2023. Overall, the present analysis concludes that the April~~ ~~2023 event had a significant impact on air quality over PSEA and its surrounding areas.~~

4. Summary and Conclusions

In April 2023, we observed an unprecedented increase in aerosol loading over the South China Sea (SCS), which had not been recorded during the two-decade MODIS satellite measurements period from 2003 to 2023. Satellite observations revealed ~150% increase in AOD (MODIS), approximately four times higher than the long-term mean, alongside significant enhancements in CO (MOPITT and AIRS) at the 700 and 500 hPa levels. This study investigates the causes, physical mechanisms, and atmospheric dynamics underlying this extraordinary aerosol

event. Analyses of satellite data (MODIS, MOPITT, AIRS, and CALIPSO), NOAA HYSPLIT back trajectories, and MERRA-2 reanalysis products indicate that intense biomass-burning activity over northern Peninsular Southeast Asia was the primary driver of the record-breaking aerosol loading over the SCS in April 2023. Our results further reveal that this BB activity was amplified by exceptional meteorological conditions associated with unusually large-scale dynamical circulation patterns. A dominant anti-cyclonic anomaly over PSEA suppressed convection, leading to subsidence, elevated surface temperatures, and drought conditions that fueled fires, particularly in Laos and Myanmar, which contributed most to the regional BB emissions. A schematic summarizing these drivers and mechanisms is presented in **Figure 11**.

Climatologically, two anti-cyclones are typically situated over the WNP and the Indian Ocean, producing predominantly southwesterly and southerly winds over the SCS. These southerly winds generally transport BB smoke from PSEA to downwind regions such as Taiwan and the WNP. In April 2023, however, the WNP anticyclone transformed into a cyclone, while the Indian Ocean anticyclone shifted eastward over the BoB near PSEA. The resulting northerly flow over the SCS, combined with easterly anomalies near Taiwan, blocked transport toward the northwestern Pacific and redirected smoke from PSEA to the SCS and BoB. This circulation shift, driven by the combined WNP cyclone and BoB anticyclone, highlights the critical role of large-scale atmospheric dynamics in determining BB smoke pathways. These findings improve understanding of transboundary pollution and can inform regional monitoring efforts over PSEA.

Formatted: Font: Bold

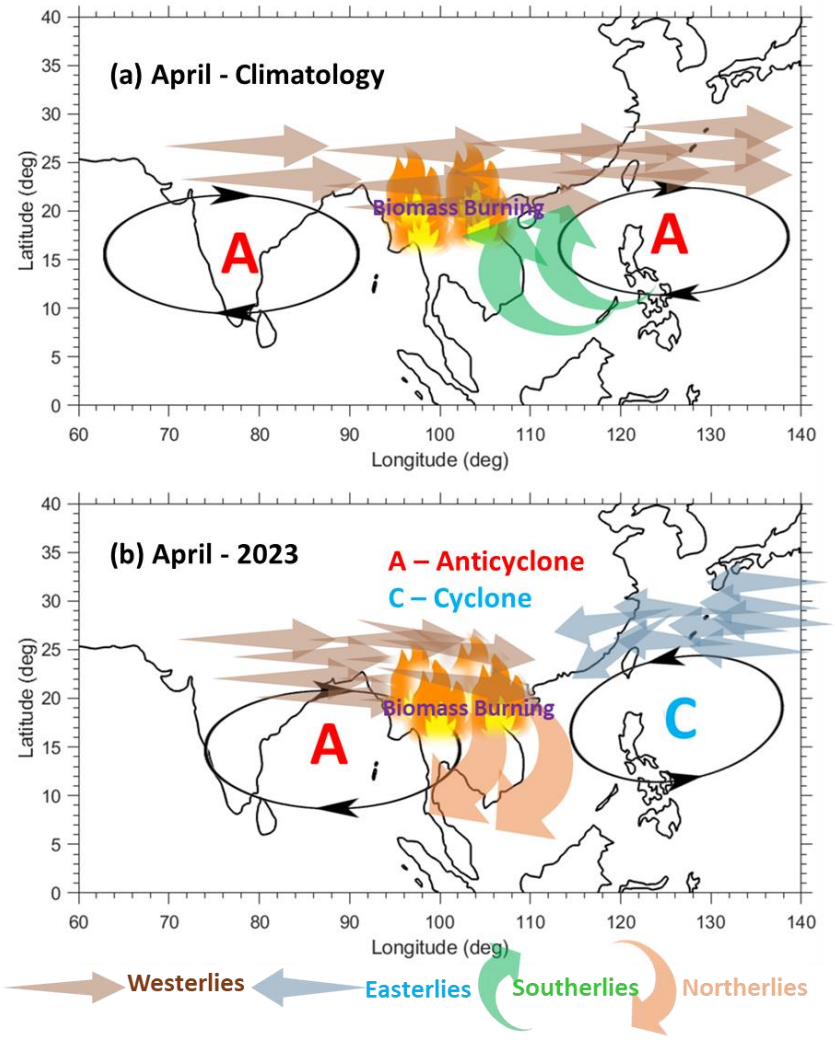

Figure 11. The schematic diagram illustrates the physical mechanisms responsible for the record-breaking aerosol loading over the South China Sea in April 2023.

The schematic illustrates the anomalous circulation and transport pathways responsible for the record aerosol loading over the South China Sea (SCS). A denotes the presence of an anticyclone anomaly, and C represents the presence of a cyclone anomaly. The horizontal arrows indicate subtropical free-tropospheric westerlies and easterlies. The green arrow indicates southerlies, and

northerlies are shown by the brown arrow, respectively. **Top panel**: climatological April (1991–2020), showing the Bay of Bengal (BoB) and western Pacific anticyclones, southwesterly and southerly winds over the SCS, and typical northward smoke transport toward Taiwan and the western North Pacific. **Bottom panel**: April 2023 anomalies, with a pronounced PSEA anticyclone, a western North Pacific cyclone, and an eastward-shifted BoB anticyclone. These anomalies generate persistent northerlies over the SCS, suppress eastward transport, and redirect biomass-burning plumes southward toward the SCS and southern BoB. Subsidence and reduced convection over PSEA enhanced surface warming and drought, favoring intense fires. Strengthened easterlies around Taiwan further inhibited northward export, producing the exceptional aerosol accumulation observed in April 2023.

While the present study focuses on the record-breaking aerosol loading, its sources, transport pathways, and dynamical drivers, the broader impacts of this extreme event remain largely unexplored. In particular, aerosol-radiation interactions associated with such unusually high AOD could substantially affect regional energy balance, atmospheric heating profiles, and the hydrological cycle over adjacent regions. Future research will aim to quantify the radiative forcing of these extreme aerosol concentrations and assess their broader atmospheric impacts. Additionally, the exceptional increase in CO and other BB emissions may have strong implications for tropospheric ozone formation, which will also be investigated. Interestingly, PSEA experienced an extreme heatwave in April 2023, with record-high temperatures (Zachariah et al., 2024; Lyu et al., 2024). Previous studies have attributed this heatwave to climate change (Zachariah et al., 2024), as well as strengthened high-pressure systems, moisture deficits, and strong land–atmosphere coupling (Lyu et al., 2024). Our results suggest a plausible contribution from biomass-burning aerosols and associated greenhouse gases to this heatwave. Key questions for future investigation include: How do greenhouse gases released by record-breaking BB activity influence regional heat trapping? What is the impact of elevated aerosol concentrations on surface radiation, cloud formation, and precipitation patterns? Addressing these questions will be critical to understanding the exceptional conditions in PSEA and surrounding regions, including the combined effects of BB aerosols and greenhouse gas emissions on regional climate extremes.

~~In April 2023, we observed an unprecedented increase in aerosol loading over the South China Sea (SCS), which had not been observed in the past two decades of the MODIS period, spanning from 2003 to 2023. Satellite observations revealed a 150% rise in aerosol optical depth~~

~~(MODIS), alongside 50% increases in carbon monoxide (MOPITT) at 700 and 500 hPa over SCS. This study primarily focused on analyzing the drivers, physical and dynamical mechanisms behind the record-breaking aerosol loading over the SCS in April 2023. Our findings indicate that extreme biomass burning (BB) activity over northern PSEA was the primary source of the record-breaking aerosols in April 2023.~~

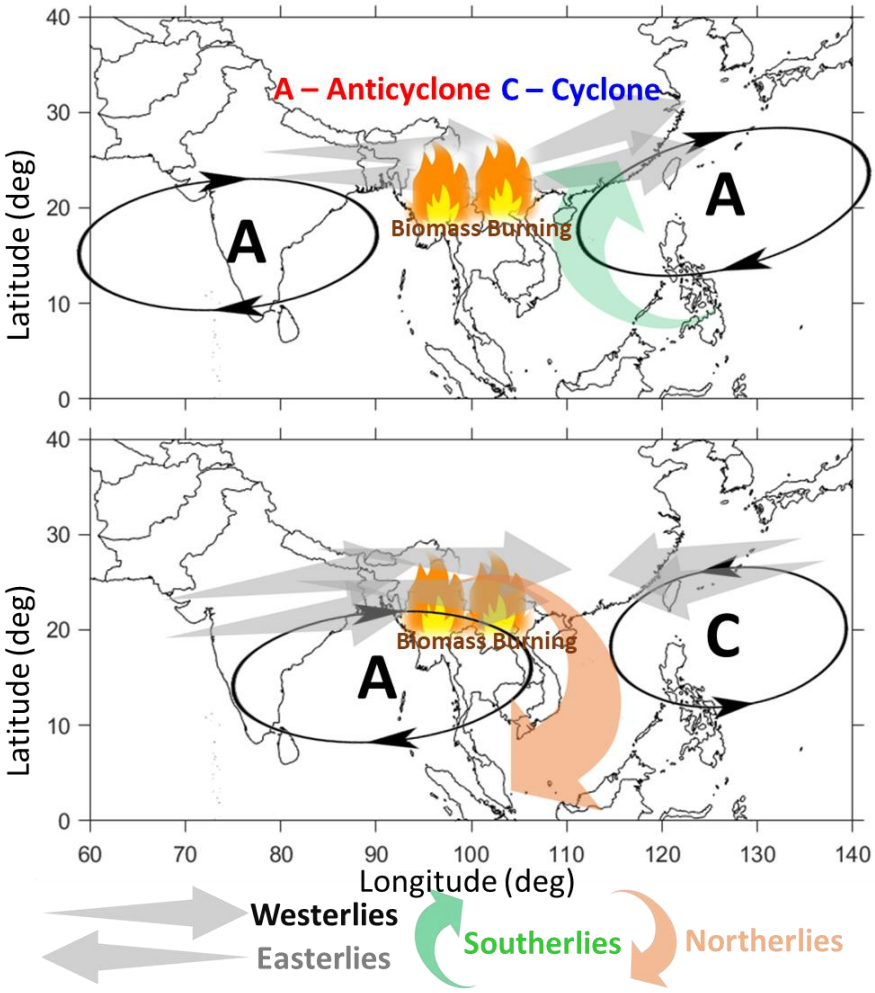

Figure 8. The schematic diagram illustrates the physical mechanisms responsible for the record-breaking aerosol loading over the South China Sea in April 2023. The top panel displays the long-term mean state in April, whereas the bottom panel shows the April 2023 mean state of the large-scale dynamical and circulatory systems. A denotes the presence of an anticyclone anomaly, and C represents the presence of a cyclone anomaly. The horizontal arrows indicate subtropical free-tropospheric westerlies and easterlies. The green arrow indicates southerlies, and northerlies are shown by the brown arrow, respectively. Two anticyclone systems were present in climatology over the western Pacific and the Indian Ocean. Southwesterly and southerly winds in the free troposphere dominate the SCS. Free tropospheric westerlies transport smoke into the downwind areas of Taiwan and the western North Pacific. In April 2023, the western North Pacific anticyclone transitioned into an anomalous cyclone over the western North Pacific. The Indian anticyclone system further shifted eastward around the PSEA. Unusual northerly winds replaced the southerly winds due to a cyclone anomaly over the western North Pacific and an expanded Indian anticyclone. Additionally, in April 2023, easterlies around Taiwan and above hindered downwind transport to the northwestern Pacific.

An analysis of various meteorological and atmospheric factors reveals that the PSEA region has experienced unusual weather patterns, creating conditions conducive to BB and wildfires. Key contributors include extremely low soil moisture, higher surface temperatures, lower precipitation levels, and an upper tropospheric high-pressure anticyclone. These factors increase the likelihood of severe fire events, especially in Laos and Myanmar. Particularly, Laos became one of the hotspot regions for extreme BB activity in April 2023. Among all the countries in PSEA, Laos alone contributed approximately 56% of the total fire activity over PSEA, followed by Myanmar at around 33%. Under prolonged dry conditions, BB activity over Laos in April 2023 was higher than in the past two decades. The largest area burned, 1.08 million hectares, in a single month (2002-2023), occurred in April 2023. Additionally, unusually large-scale atmospheric circulations significantly spread smoke, trace gases, and pollutants to downwind regions from the source. Our analysis of large-scale circulations associated with dynamical changes illustrates the mechanism behind the April 2023 event, as schematically shown in **Figure 8**. In climatology, two anticyclone systems were situated over the WNP and the Indian Ocean. The SCS experiences predominantly southwesterly and southerly winds in the free troposphere. Westerly winds in the free troposphere generally transport BB smoke from PSEA to downwind areas of Taiwan and the WNP. In April 2023, the anticyclone over the WNP transformed into an unusual cyclone. Meanwhile, the Indian anticyclone shifted eastward over the BoB and near the PSEA. Due to a cyclone anomaly in the WNP and a persistent anticyclone in the BoB, northerly winds replaced the southerly winds in the free troposphere over the SCS. Additionally, in April 2023, easterlies near Taiwan obstructed downwind transport towards the northwestern Pacific. Overall, it is concluded that the regime

~~shifted from southerlies to northerlies over the SCS due to the combined impact of the extended BoB anticyclone and the WNP cyclone, causing BB smoke transport from the PSEA to the SCS. The present findings would benefit regional monitoring and a better understanding of the transboundary pollution over the PSEA.~~

~~Interestingly, PSEA is linked to an extreme heatwave in April 2023, with record high temperatures (Zachariah et al., 2024; Lyu et al., 2024). Studies have attributed this heatwave to climate change (Zachariah et al., 2024), as well as to the strengthening of high pressure from tropical waves, moisture deficiency, and strong land-atmosphere coupling (Lyu et al., 2024). Our results further suggest a plausible role for BB-associated aerosols and greenhouse gases in the April 2023 heatwave. What role does heat trapping play in increasing greenhouse gases resulting from record-breaking BB activity? What is the impact of increased BB aerosols? Further research is needed to understand the exceptional conditions in PSEA and its surrounding regions, including BB-associated greenhouse gas emissions (GHGs) and aerosol anomalies. Additionally, smoke aerosols impact surface and atmospheric radiation budgets, affecting regional weather and climate. Future work will focus on the radiative energy balance and weather changes resulting from the April 2023 aerosol increase.~~

Data availability

MODIS data available from https://modis.gsfc.nasa.gov/data/dataprod/mod08.php. The AIRS and MOPITT CO data can be downloaded from https://disc.gsfc.nasa.gov/datasets/AIRS3STM_7.0 (AIRS project, 2019) and https://asdc.larc.nasa.gov/project/MOPITT/MOP02J_8 (NASA, 2023a). MERRA-2 data are available online through the NASA Goddard Earth Sciences Data Information Services Center (GES DISC; https://disc.gsfc.nasa.gov; NASA, 2023b). The MODIS fire and burned area products can be downloaded from https://firms.modaps.eosdis.nasa.gov/active_fire/ (NASA, 2023c). Daily CALIPSO vertical distribution images of various aerosol types were obtained from https://www-calipso.larc.nasa.gov/products. The NOAA HYSPLIT back trajectories are retrieved from https://www.ready.noaa.gov/HYSPLIT.php. /~~The OMI/MLS tropospheric column ozone data can be obtained from https://acd-ext.gsfc.nasa.gov/Data_services/cloud_slice/ (last access 01 July 2025).~~

Author Contributions

Saginela Ravindra Babu: Conceptualization, Data curation, Formal analysis, Investigation, Software, Validation, Visualization, Writing – original draft preparation, Writing – review and editing; **Neng-Huei Lin**: Conceptualization, Investigation, Funding Acquisition, Supervision, Resources, Writing – review and editing.

Competing interests

The authors declare no competing interests.

Acknowledgements

We acknowledge the National Science and Technology Council of Taiwan for supporting the research. The authors thank NASA and NOAA for providing MOPITT, MODIS, CALIPSO and AIRS satellite data. We thank NASA's Global Monitoring and Assimilation Office (GMAO) for providing the Modern-Era Retrospective analysis for Research and Applications, Version 2 (MERRA-2) data.

References

Seneviratne, S. I. et al. Weather and Climate Extreme Events in a Changing Climate. In Proc. Climate Change 2021: The Physical Science Basis. Contribution of Working Group I to the Sixth Assessment Report of the Intergovernmental Panel on Climate Change, 1513–1766 (Cambridge University Press, 2021). https://doi.org/10.1017/9781009157896.013.

Esper, J., Torbenson, M. & Büntgen, U. 2023 summer warmth unparalleled over the past 2,000 years. Nature 631, 94–97 (2024). https://doi.org/10.1038/s41586-024-07512-y

Forster, P. M. et al. Indicators of Global Climate Change 2023: annual update of key indicators of the state of the climate system and human influence. Earth Syst. Sci. Data 16, 2625–2658 (2024). https://doi.org/10.5194/essd-16-2625-2024

Formatted: No underline
Formatted: No underline
Formatted: No underline
Formatted: No underline
Formatted: No underline
Formatted: No underline
Formatted: No underline

Min, S. K. Human influence can explain the widespread exceptional warmth in 2023. Commun. Earth Environ. 5, 215 (2024). https://doi.org/10.1038/s43247-024-01391-x

Perkins-Kirkpatrick, S., Barriopedro, D., Jha, R. et al. Extreme terrestrial heat in 2023. Nat Rev Earth Environ 5, 244–246 (2024). https://doi.org/10.1038/s43017-024-00536-y

Raghuraman, S. P. et al. The 2023 global warming spike was driven by the El Niño–Southern Oscillation. Atmos. Chem. Phys. 24, 11275–11283 (2024). https://doi.org/10.5194/acp-24-11275-2024

Kolden, C. A., Abatzoglou, J. T., Jones, M. W. & Jain, P. Wildfires in 2023. Nat. Rev. Earth Environ. 5, 238–240 (2024).

Liu, Z., Deng, Z., Davis, S. J. et al. Global carbon emissions in 2023. Nat. Rev. Earth Environ. 5, 253–254 (2024). https://doi.org/10.1038/s43017-024-00532-2

Byrne, B., Liu, J., Bowman, K. W. et al. Carbon emissions from the 2023 Canadian wildfires. Nature 633, 835–839 (2024). https://doi.org/10.1038/s41586-024-07878-z

MacCarthy, J., Tyukavina, A., Weisse, M. J., Harris, N. & Glen, E. Extreme wildfires in Canada and their contribution to global loss in tree cover and carbon emissions in 2023. Glob. Change Biol. 30, e17392 (2024). https://doi.org/10.1111/gcb.17392

Jain, P., Barber, Q.E., Taylor, S.W. et al. Drivers and Impacts of the Record-Breaking 2023 Wildfire Season in Canada. Nature Commun. 15, 6764 (2024). https://doi.org/10.1038/s41467-024-51154-7

Lai, G. & Zhang Y. Increased atmospheric aridity and reduced precipitation drive the 2023 extreme wildfire season in Canada. Geophy. Res. Lett., 52, e2024GL114492 (2025). https://doi.org/10.1029/2024GL114492

Liu, G., Li, J. Li X. & Ying T. North Atlantic and the Barents Sea variability contribute to the 2023 extreme fire season in Canada. Proc. Natl. Acad. Sci. USA, 121 (49) e2414241121 (2024). https://doi.org/10.1073/pnas.2414241121

Roy, D. P., De Lemos, H., Huang, H., Giglio, L., Houborg, R. & Miura, T. Multi-resolution monitoring of the 2023 Maui wildfires, implications and needs for satellite-based wildfire disaster monitoring. Sci. Remote Sens. 10, 100142 (2024). https://doi.org/10.1016/j.srs.2024.100142

Lemus-Canovas, M., Insua-Costa, D., Trigo, R. M. & Miralles, D. G. Record-shattering 2023 Spring heatwave in western Mediterranean amplified by long-term drought. Npj Clim. Atmos. Sci. 7, 25 (2024). https://doi.org/10.1038/s41612-024-00569-6.

Espinoza, J. C. et al. The new record of drought and warmth in the Amazon in 2023 related to regional and global climatic features. Sci. Rep. 14, 8107 (2024). https://doi.org/10.1038/s41598-024-58782-5

Formatted: No underline
Formatted: No underline
Formatted: Font: (Default) Times New Roman, 12 pt, No underline
Formatted: No underline
Formatted: No underline
Formatted: No underline
Formatted: No underline
Formatted: No underline
Formatted: No underline
Formatted: Font: (Default) Times New Roman, 12 pt, No underline
Formatted: No underline
Formatted: No underline
Formatted: No underline
Formatted: No underline
Formatted: No underline
Formatted: No underline
Formatted: No underline
Formatted: No underline
Formatted: No underline
Formatted: No underline
Formatted: Font: (Default) Times New Roman, 12 pt, No underline
Formatted: No underline
Formatted: No underline
Formatted: No underline
Formatted: No underline

~~Jones, M. W. et al. State of wildfires 2023–2024. Earth Syst. Sci. Data 16, 3601–3685 (2024). https://doi.org/10.5194/essd-16-3601-2024~~

~~Cordero, R.R., Feron, S., Damiani, A. et al. Extreme fire weather in Chile driven by climate change and El Niño–Southern Oscillation (ENSO). Sci Rep 14, 1974 (2024). https://doi.org/10.1038/s41598-024-52481-x~~

~~Michailidis, K. et al. Extreme wildfires over northern Greece during summer 2023 – part A: Effects on aerosol optical properties and solar UV radiation. Atmos. Res. 311, 107700 (2024). https://doi.org/10.1016/j.atmosres.2024.~~

~~NOAA NCE, 2023. National oceanic and atmospheric administration (NOAA) national centers for environmental information (NCE), September 11th 2023. "U.S. Billion- dollar weather and climate disasters 1980-2023 report". Available online at: https://www.ncei.noaa.gov/access/billions/events.pdf~~

~~Ke, P. et al. Low latency carbon budget analysis reveals a large decline of the land carbon sink in 2023. Natl. Sci. Rev. 11, nwae367 (2024). https://doi.org/10.1093/nsr/nwae367~~

~~Gui, Y. et al. The decline in tropical land carbon sink drives high atmospheric CO_2 growth rate in 2023. Natl. Sci. Rev. nwae365 (2024). https://doi.org/10.1093/nsr/nwae365~~

~~Xia, L., Liu, R., Fan, W. et al. Emerging carbon dioxide hotspots in East Asia identified by a top-down inventory. Commun Earth Environ 6, 10 (2025). https://doi.org/10.1038/s43247-024-01991-7~~

~~Pani, S.K. et al. Long-term observation of columnar aerosol optical properties over the remote South China Sea. Sci. Total Environ. 905, 167113 (2023). https://doi.org/10.1016/j.scitotenv.2023.167113~~

~~Buchholz, R. R. et al. Air pollution trends measured from Terra: CO and AOD over industrial, fire-prone, and background regions. Remote Sensing Environ. 256, 112275 (2021). https://doi.org/10.1016/j.rse.2020.112275~~

~~Cui, D.Y. et al. Impact of atmospheric wet deposition on phytoplankton community structure in the South China Sea. Estuar. Coast. Shelf Sci. 173, 1–8 (2016). https://doi.org/10.1016/j.ecss.2016.02.011~~

~~Lin, N. H. et al. An overview of regional experiments on biomass burning aerosols and related pollutants in Southeast Asia: from BASE-ASIA and the Dongsha Experiment to 7-SEAS. Atmos. Environ. 78, 1–19 (2013). https://doi.org/10.1016/j.atmosenv.2013.04.066~~

~~Reid, J. S. et al. Observing and understanding the Southeast Asian aerosol system by remote sensing: an initial review and analysis for the Seven Southeast Asian Studies (7SEAS) program. Atmos. Res. 122, 403–468 (2013). https://doi.org/10.1016/j.atmosres.2012.06.005~~

Formatted: No underline
Formatted: No underline
Formatted: No underline
Formatted: No underline
Formatted: No underline
Formatted: No underline
Formatted: No underline
Formatted: No underline
Formatted: Font: (Default) Times New Roman, 12 pt, No underline
Formatted: No underline
Formatted: No underline
Formatted: No underline
Formatted: No underline
Formatted: No underline
Formatted: No underline
Formatted: No underline
Formatted: Font: (Default) Times New Roman, 12 pt, No underline
Formatted: No underline
Formatted: No underline
Formatted: No underline
Formatted: Font: (Default) Times New Roman, 12 pt, No underline
Formatted: No underline
Formatted: No underline
Formatted: No underline
Formatted: No underline
Formatted: Font: (Default) Times New Roman, 12 pt, No underline
Formatted: No underline
Formatted: No underline

Lee, C. T. et al. Aerosol chemical profile of near-source biomass burning smoke in Sonla, Vietnam during 7-SEAS campaigns in 2012 and 2013. Aerosol Air Qual. Res. 16, 2603–2617 (2016). https://doi.org/10.4209/aaqr.2015.07.0465

Tsay, S. C. et al. Satellite-surface perspectives of air quality and aerosol-cloud effects on the environment: An overview of 7-SEAS/BASELInE. Aerosol Air Qual. Res. 16, 2581–2602 (2016). https://doi.org/10.4209/aaqr.2016.08.0350

Huang, H. Y. et al. Influence of synoptic-dynamic meteorology on the long-range transport of Indochina biomass burning aerosols. J. Geophys. Res. Atmos. 125, e2019JD031260 (2020). https://doi.org/10.1029/2019JD031260

Ou-Yang, C.F. et al. Detection of stratospheric intrusion events and their role in ozone enhancement at a mountain background site in sub-tropical East Asia. Atmos. Environ. 268, 118779 (2022). https://doi.org/10.1016/j.atmosenv.2021.118779

Alexander, L. Extreme heat rooted in dry soils. Nature Geosci 4, 12–13 (2011). https://doi.org/10.1038/ngeo1045

Fischer, E. M., Seneviratne, S. I., Vidale, P. L., Lüthi, D. & Schär, C. M. Soil Moisture–Atmosphere Interactions during the 2003 European Summer Heat Wave. J. Clim. 20, 5081–5099 (2007). https://doi.org/10.1175/JCLI4288.1

Dong, Z., Yang, R., Cao, J., Wang, L. & Cheng, J. A strong high-temperature event in late spring 2023 in Yunnan province, Southwest China: Characteristics and possible causes. Atmos. Res 295, 107017 (2023). https://doi.org/10.1016/j.atmosres.2023.107017

Ma, T. et al. Attribution analysis of the persistent and extreme drought in southwest China during 2022–2023. Environ. Res. Lett. 19, 114056 (2024).

Wai, K. M., Lin, N. H., Wang, S. H., and Dokiya, Y. Rainwater chemistry at a high altitude station, Mt. Lulin, Taiwan: comparison with a background station, Mt. Fuji, J. Geophy. Res. 113, D06305 (2008). doi:10.1029/2006JD008248.

Lin, C. Y. et al. A new transport mechanism of biomass burning from Indochina as identified by modeling studies. Atmos. Chem. Phys. 9, 7901–7911 (2009). https://doi.org/10.5194/acp-9-7901-2009

Chuang, M.T. et al. Carbonaceous aerosols in the air masses transported from Indochina to Taiwan: Long-term observation at Mt. Lulin. Atmos. Environ. 89, 507–516 (2014). https://doi.org/10.1016/j.atmosenv.2013.11.066

Lin, C.C. et al. Influences of the long-range transport of biomass-burning pollutants on surface air quality during 7-SEAS field campaigns. Aerosol Air Qual. Res. 17, 2595–2607 (2017). https://doi.org/10.4209/aaqr.2017.08.0273

Formatted: No underline
Formatted: No underline
Formatted: Font: (Default) Times New Roman, 12 pt, No underline
Formatted: No underline
Formatted: No underline
Formatted: No underline
Formatted: No underline
Formatted: No underline
Formatted: No underline
Formatted: No underline
Formatted: No underline
Formatted: No underline
Formatted: No underline
Formatted: No underline
Formatted: No underline
Formatted: No underline
Formatted: No underline
Formatted: No underline
Formatted: No underline
Formatted: No underline
Formatted: No underline
Formatted: No underline
Formatted: No underline

~~Ou-Yang, C.F. et al. Characteristics of atmospheric carbon monoxide at a high-mountain background station in East Asia. Atmos. Environ. 89, 613–622 (2014). https://doi.org/10.1016/j.atmosenv.2014.02.060~~

~~Pani, S.K. et al. Relationship between long-range transported atmospheric black carbon and carbon monoxide at a high-altitude background station in East Asia. Atmos. Environ. 210, 86–99 (2019). https://doi.org/10.1016/j.atmosenv.2019.04.053~~

~~Ravindra Babu, S. et al. Transport pathways of carbon monoxide from Indonesian fire pollution to a subtropical high-altitude mountain site in the western North Pacific. Atmos. Chem. Phys. 23, 4727–4740 (2023). https://doi.org/10.5194/acp-23-4727-2023~~

~~Huang, H. Y. et al. Impact of regional climate patterns on the biomass burning emissions and transport over Peninsular Southeast Asia, 2000–2019. Atmos. Res. 297, 107067 (2024). https://doi.org/10.1016/j.atmosres.2023.107067~~

~~Hu, Y., Yue, X. & Tian, C. Climatic drivers of the Canadian wildfire episode in 2023. Atmos. Oceanic Sci. Lett. 17, 100483 (2024). https://doi.org/10.1016/j.aosl.2024.100483~~

~~Sheu G. R., N. H. Lin, J. L. Wang, C. T. Lee. Temporal distribution and potential sources of atmospheric mercury measured at a high-elevation background station in Taiwan. Atmos. Environ. 44, 2393–2400 (2010).~~

~~Gill, A. E. Some simple solutions for heat-induced tropical circulation. Q. J. R. Meteorol. Soc. 106, 447–462 (1980). https://doi.org/10.1002/qj.49710644905~~

~~Zeng, Z. & Sun, J. Impacts of a tripolar sea surface temperature pattern over tropical–North Pacific on interannual variations of spring extreme consecutive dry days over southern China. J. Geophys. Res. Atmos. 127, e2021JD036281 (2022). https://doi.org/10.1029/2021JD036281~~

~~Jaffe, D. A. & Wigder, N. L. Ozone production from wildfires: a critical review. Atmos. Environ. 51, 1–10 (2012). https://doi.org/10.1016/j.atmosenv.2011.11.063~~

~~Ogino, S. Y. et al. Cause of a lower-tropospheric high-ozone layer in spring over Hanoi. J. Geophys. Res. Atmos. 127, e2021JD035727 (2022). https://doi.org/10.1029/2021JD035727~~

~~Liu, H. et al. Sources of tropospheric ozone along the Asian Pacific Rim: An analysis of ozonesonde observations. J. Geophys. Res. 107, ACH31 ACH319 (2002). https://doi.org/10.1029/2001JD002005~~

~~Chan, C.Y. et al. Characteristics of biomass burning emission sources, transport, and chemical speciation in enhanced springtime tropospheric ozone profile over Hong Kong. J. Geophys. Res. 108, 1 (2003). https://doi.org/10.1029/2001jd001555~~

~~Ou-Yang, C.F. et al. Seasonal and diurnal variations of ozone at a high-altitude mountain baseline station in East Asia. Atmos. Environ. 46, 279–288 (2012). https://doi.org/10.1016/j.atmosenv.2011.09.060~~

Formatted: No underline
Formatted: No underline
Formatted: No underline
Formatted: No underline
Formatted: No underline
Formatted: No underline
Formatted: No underline
Formatted: No underline
Formatted: No underline
Formatted: No underline
Formatted: No underline
Formatted: No underline
Formatted: No underline
Formatted: No underline
Formatted: No underline
Formatted: No underline
Formatted: No underline
Formatted: No underline
Formatted: No underline
Formatted: No underline
Formatted: No underline
Formatted: No underline
Formatted: No underline
Formatted: No underline
Formatted: No underline
Formatted: No underline
Formatted: No underline
Formatted: No underline
Formatted: No underline
Formatted: No underline
Formatted: No underline
Formatted: No underline
Formatted: No underline

Yadav, I.C. et al. Biomass burning in Indo-China peninsula and its impacts on regional air quality and global climate change a review. Environ. Pollut. 227, 414–427 (2017). https://doi.org/10.1016/j.envpol.2017.04.085

Liao, Z. et al. Tropospheric ozone variability over Hong Kong based on recent 20-year (2000–2019) ozonesonde observation. J. Geophys. Res. Atmos. 126, e2020JD033054 (2021). https://doi.org/10.1029/2020jd033054

Zachariah, M. et al. Extreme humid heat in South and Southeast Asia in April 2023, largely driven by climate change, detrimental to vulnerable and disadvantaged communities. World Weather Attribution (2023). Available at: https://spiral.imperial.ac.uk/bitstream/10044/1/104092/18/south%20asia%20heat%20scientific%20report.pdf

Lyu, Y. et al. The characterization, mechanism, predictability, and impacts of the unprecedented 2023 Southeast Asia heatwave. npj Clim. Atmos. Sci. 7, 246 (2024). https://doi.org/10.1038/s41612-024-00797-w

Platnick, S., King, M. & Hubanks, P. MODIS Atmosphere L3 Monthly Product. https://doi.org/10.5067/MODIS/MOD08_M3.006 (2015).

Buchholz, R. R. et al. Air pollution trends measured from Terra: CO and AOD over industrial, fire-prone, and background regions. Remote Sensing Environ. 256, 112275 (2020). https://doi.org/10.1016/j.rse.2020.112275

Giglio, L., Csiszar, I. & Justice, C. O. Global distribution and seasonality of active fires as observed with the Terra and Aqua MODIS sensors. J. Geophys. Res. Biogeosci. 111, G02016 (2006). https://doi.org/10.1029/2005JG000142

Giglio, L., Schroeder, W. & Justice, C. O. The Collection 6 MODIS active fire detection algorithm and fire products. Remote Sens. Environ. 178, 31–41 (2016). https://doi.org/10.1016/j.rse.2016.02.054

Giglio, L., Boschetti, L., Roy, D. P., Humber, M. L. & Justice, C. O. The Collection 6 MODIS burned area mapping algorithm and product. Remote Sens. Environ. 217, 72–85 (2018). https://doi.org/10.1016/j.rse.2018.08.005

Worden, H. M. et al. Observations of near-surface carbon monoxide from space using MOPITT multispectral retrievals. J. Geophys. Res.: Atmos. 115, (2010). https://doi.org/10.1029/2010JD014242

Deeter, M. N. et al. Radiance-based retrieval bias mitigation for the MOPITT instrument: the version 8 product. Atmos. Meas. Tech. 12, 4561–4580 (2019). https://doi.org/10.5194/amt-12-4561-2019

McMillan, W. W. et al. Daily global maps of carbon monoxide from NASA's Atmospheric Infrared Sounder. Geophys. Res. Lett. 32 (2005). https://doi.org/10.1029/2004GL021821

Formatted: No underline

~~Warner, J. X. et al. A comparison of satellite tropospheric carbon monoxide measurements from AIRS and MOPITT during INTEX-A. J. Geophys. Res. 112, D12S17 (2007). https://doi.org/10.1029/2006JD007925~~

~~Warner, J. et al. Tropospheric carbon monoxide variability from AIRS under clear and cloudy conditions. Atmos. Chem. Phys. 13, 12469–12479 (2013). https://doi.org/10.5194/acp-13-12469-2013~~

~~McMillan, W. W. et al. Validating the AIRS Version 5 CO retrieval with DACOM in situ measurements during INTEX-A and -B. IEEE Trans. Geosci. Remote Sens. 49, 2802–2813 (2011). https://doi.org/10.1109/TGRS.2011.2106505~~

~~AIRS Project. Aqua/AIRS L3 Monthly Standard Physical Retrieval (AIRS only) 1 degree × 1 degree V7.0. Goddard Earth Sciences Data and Information Services Center (GES DISC), Greenbelt, MD, USA (2019). https://doi.org/10.5067/UBENJB9D3T2H~~

~~Ziemke, J. R. et al. Trends in global tropospheric ozone inferred from a composite record of TOMS/OMI/MLS/OMPS satellite measurements and the MERRA-2 GMI simulation. Atmos. Chem. Phys. 19, 3257–3269 (2019). https://doi.org/10.5194/acp-19-3257-2019~~

~~Ziemke, J. R. et al. Tropospheric ozone determined from Aura OMI and MLS: evaluation of measurements and comparison with the Global Modeling Initiative's Chemical Transport Model. J. Geophys. Res. 111, D19303 (2006). https://doi.org/10.1029/2006JD007089.~~

~~Cooper, O. R. et al. Increasing springtime ozone mixing ratios in the free troposphere over western North America. Nature 463, 344–348 (2010). https://doi.org/10.1038/nature08708~~

~~Gaudel, A. et al. Tropospheric Ozone Assessment Report: Present-day distribution and trends of tropospheric ozone relevant to climate and global atmospheric chemistry model evaluation. Elem. Sci. Anth. 6, 39 (2018). https://doi.org/10.1525/elementa.291~~

~~Lu, et al. An evaluation of the ability of the Ozone Monitoring Instrument (OMI) to observe boundary layer ozone pollution across China: application to 2005–2017 ozone trends. Atmos. Chem. Phys. 19, 6551–6560 (2019). https://doi.org/10.5194/acp-19-6551-2019~~

~~Gelaro, R. et al. The modern-era retrospective analysis for research and applications, Version 2 (MERRA-2). J. Clim. 30, 5419–5454 (2017). https://doi.org/10.1175/JCLI-D-16-0758.1~~Anderson, T. L., Charlson, R. J., Schwartz, S. E., Knutti, R., Boucher, O., Rodhe, H., and Heintzenberg, J.: Climate forcing by aerosol– a hazy picture, Science, 300, 1103–1104, https://doi.org/10.1126/science.1084777, 2003.

AIRS Project. Aqua/AIRS L3 Monthly Standard Physical Retrieval (AIRS-only) 1 degree x 1 degree V7.0 [Data set]. NASA Goddard Earth Sciences Data and Information Services Center. https://doi.org/10.5067/UBENJB9D3T2H, 2020.

Buchholz, R. R., Worden, H. M., Park, M., Francis, G., Deeter, M. N., Edwards, D. P., Emmons, L. K., Gaubert, B., Gille, J., Martinez-Alonso, S., Tang, W., Kumar, R., Drummond, J. R., Clerbaux, C., George, M., Coheur, P.-F., Hurtmans, D., Bowman, K. W., Luo, M., Payne, V. H.,

Formatted: No underline
Formatted: No underline
Formatted: No underline
Formatted: No underline
Formatted: No underline
Formatted: No underline
Formatted: No underline
Formatted: No underline
Formatted: No underline
Formatted: No underline
Formatted: No underline
Formatted: No underline
Formatted: No underline
Formatted: No underline
Formatted: No underline
Formatted: No underline
Formatted: No underline
Formatted: No underline
Formatted: No underline
Formatted: No underline
Formatted: No underline
Formatted: No underline
Formatted: No underline
Formatted: No underline
Formatted: No underline
Formatted: No underline
Formatted: No underline
Formatted: No underline, Font color: Auto
Formatted: No underline, Font color: Auto
Formatted: No underline, Font color: Auto

Worden, J. R., Chin, M., Levy, R. C., Warner, J., Wei, Z., and Kulawik, S. S.: Air pollution trends measured from Terra: CO and AOD over industrial, fire-prone, and background regions, Remote Sens. Environ., 256, 112275, https://doi.org/10.1016/j.rse.2020.112275, 2021.

Byrne, B., Liu, J., and Bowman, K. W.: Carbon emissions from the 2023 Canadian wildfires, Nature, 633, 835–839, https://doi.org/10.1038/s41586-024-07878-z, 2024.

Chan, C. Y., Chan, L. Y., Harris, J. M., Oltmans, S. J., Blake, D. R., Qin, Y., Zheng, Y. G., and Zheng, X. D.: Characteristic of biomass burning emission sources, transport, and chemical speciation in enhanced springtime tropospheric ozone profile over Hong Kong, J. Geophys. Res., 108, 4015, https://doi.org/10.1029/2001JD001555, 2003.

Chang, J. H.-W., Wong, Y. J., Ooi, M. C.-G., Babu, S. R., Pani, S. K., and Lin, N.-H.: Biomass burning in critical fire region over the Maritime Continent from 2012 to 2021: A review of the meteorological influence and cloud-aerosol-radiation interactions, Atmos. Environ., 320, 120324, https://doi.org/10.1016/j.atmosenv.2023.120324, 2024.

Chuang, M-T., Lee, C-T., Chou, C. C-K., Lin, N-H., Sheu, G-R., Wang, J-L., Chang, S-C., Wang, S-H., Chi, K. H., Young, C-Y., Huang, H., Chen, H-W., Weng, G-H., Lai, S-Y., Hsu, S-P., Chang, Y-J., Chang, J-H., and Wu, X-C.: Carbonaceous aerosols in the air masses transported from Indochina to Taiwan: Longterm observation at Mt. Lulin, Atmos. Environ., 89, 507–516, https://doi.org/10.1016/j.atmosenv.2013.11.066, 2014.

Cohen, J. B.: Quantifying the occurrence and magnitude of the Southeast Asian fire climatology, Environ. Res. Lett., 9, 114018, https://doi.org/10.1088/1748-9326/9/11/114018, 2014.

Cohen, J. B., Lecoeur, E., and Hui Loong Ng, D.: Decadal-scale relationship between measurements of aerosols, land-use change, and fire over Southeast Asia, Atmos. Chem. Phys., 17, 721–743, https://doi.org/10.5194/acp-17-721-2017, 2017.

Cordero, R. R., Feron, S., Damiani, A., Carrasco, J., Karas, C., Wang, C., Kraamwinkel, C. T., and Beaulieu, A.: Extreme fire weather in Chile driven by climate change and El Niño–Southern Oscillation (ENSO), Sci. Rep., 14, 1974, https://doi.org/10.1038/s41598-024-52481-x, 2024.

Cui, D., Wang, J., Tan, L., and Dong, Z.: Impact of atmospheric wet deposition on phytoplankton community structure in the South China Sea. Estuar. Coast. Shelf Sci. 173: 1–8, https://doi.org/10.1016/j.ecss.2016.02.011, 2016.

Crutzen, P. J. and Andreae, M. O.: Biomass Burning in the Tropics: Impact on Atmospheric Chemistry and Biogeochemical Cycles, Science, 250, 1669–1678, https://doi.org/10.1126/science.250.4988.1669, 1990.

Deeter, M. N., Edwards, D. P., Francis, G. L., Gille, J. C., Mao, D., Martínez-Alonso, S., Worden, H. M., Ziskin, D., and Andreae, M. O.: Radiance-based retrieval bias mitigation for the MOPITT

Formatted: Font: Not Bold

Formatted: No underline, Font color: Auto

Formatted: No underline, Font color: Auto

Formatted: No underline, Font color: Auto

Formatted: No underline, Font color: Auto

Formatted: No underline, Font color: Auto

instrument: the version 8 product, Atmos. Meas. Tech., 12, 4561–4580, https://doi.org/10.5194/amt-12-4561-2019, 2019.

Dong, Z., Yang, R., Cao, J., Wang, L., and Cheng, J.: A strong high-temperature event in late-spring 2023 in Yunnan province, Southwest China: Characteristics and possible causes. Atmos. Res, 295, 107017. https://doi.org/10.1016/j.atmosres.2023.107017, 2023.

Espinoza, J.-C., Jimenez, J. C., Marengo, J. A., Schongart, J., Ronchail, J., Lavado-Casimiro, W., and Ribeiro, J. V. M.: The new record of drought and warmth in the Amazon in 2023 related to regional and global climatic features, Sci. Rep., 14, 8107, https://doi.org/10.1038/s41598-024-58782-5, 2024.

Fischer, E. M., Seneviratne, S. I., Vidale, P. L., Lüthi, D., and Schär, C.: Soil Moisture – Atmosphere Interactions during the 2003 European Summer Heat Wave, J. Climate, 20, 5081–5099, https://doi.org/10.1175/JCLI4288.1, 2007.

Forster, P., Storelvmo, T., Armour, K., Collins, W., Dufresne, J.-L., Frame, D., Lunt, D. J., Mauritsen, T., Palmer, M. D., Watanabe, M., Wild, M., and Zhang, H.: The Earth's Energy Budget, Climate Feedbacks, and Climate Sensitivity, in: Climate Change 2021: The Physical Science Basis, Contribution of Working Group I to the Sixth Assessment Report of the Intergovernmental Panel on Climate Change, edited by: Masson-Delmotte, V., Zhai, P., Pirani, A., Connors, S. L., Péan, C., Berger, S., Caud, N., Chen, Y., Goldfarb, L., Gomis, M. I., Huang, M., Leitzell, K., Lonnoy, E., Matthews, J. B. R., Maycock, T. K., Waterfield, T., Yelekçi, O., Yu, R., and Zhou, B., Cambridge University Press, Cambridge, United Kingdom and New York, NY, USA, pp. 923–1054, https://doi.org/10.1017/9781009157896.009, 2021.

Forster, P. M., Smith, C., Walsh, T., Lamb, W. F., Lamboll, R., Hall, B., Hauser, M., Ribes, A., Rosen, D., Gillett, N. P., Palmer, M. D., Rogelj, J., von Schuckmann, K., Trewin, B., Allen, M., Andrew, R., Betts, R. A., Borger, A., Boyer, T., Broersma, J. A., Buontempo, C., Burgess, S., Cagnazzo, C., Cheng, L., Friedlingstein, P., Gettelman, A., Gütschow, J., Ishii, M., Jenkins, S., Lan, X., Morice, C., Mühle, J., Kadow, C., Kennedy, J., Killick, R. E., Krummel, P. B., Minx, J. C., Myhre, G., Naik, V., Peters, G. P., Pirani, A., Pongratz, J., Schleussner, C.-F., Seneviratne, S. I., Szopa, S., Thorne, P., Kovilakam, M. V. M., Majamäki, E., Jalkanen, J.-P., van Marle, M., Hoesly, R. M., Rohde, R., Schumacher, D., van der Werf, G., Vose, R., Zickfeld, K., Zhang, X., Masson-Delmotte, V., and Zhai, P.: Indicators of Global Climate Change 2023: annual update of key indicators of the state of the climate system and human influence, Earth Syst. Sci. Data, 16, 2625–2658, https://doi.org/10.5194/essd-16-2625-2024, 2024.

Gelaro, R., McCarty, W., Su?rez, M. J., Todling, R., Molod, A., Takacs, L., Randles, C. A., Darmenov, A., Bosilovich, M. G., Reichle, R., Wargan, K., Coy, L., Cullather, R., Draper, C., Akella, S., Buchard, V., Conaty, A., da Silva, A. M., Gu, W., Kim, G.-K., Koster, R., Lucchesi, R., Merkova, D., Nielsen, J. E., Partyka, G., Pawson, S., Putman, W., Rienecker, M., Schubert, S. D., Sienkiewicz, M., and Zhao, B.: The Modern-Era Retrospective Analysis for Research and Applications, Version 2 (MERRA-2), J. Climate, 30, 5419–5454, https://doi.org/10.1175/JCLI-D-16-0758.1, 2017.

Formatted: No underline, Font color: Auto

Formatted: No underline, Font color: Auto

Giglio, L., Csiszar, I., and Justice, C. O.: Global distribution and seasonality of active fires as observed with the Terra and Aqua Moderate Resolution Imaging Spectroradiometer (MODIS) sensors, J. Geophys. Res.-Biogeo., 111, https://doi.org/10.1029/2005JG000142, 2006.

Giglio, L., Schroeder, W., and Justice, C. O.: The collection 6 MODIS active fire detection algorithm and fire products, Remote Sens. Environ., 178, 31–41, https://doi.org/10.1016/j.rse.2016.02.054, 2016.

Giglio, L., Boschetti, L., Roy, D. P., Humber, M. L., and Justice, C. O.: The Collection 6 MODIS burned area mapping algorithm and product, Remote Sens. Environ., 217, 72–85, https://doi.org/10.1016/j.rse.2018.08.005, 2018.

Gill, A. E.: Some simple solutions for heat-induced tropical circulation. Q. J. R. Meteorol. Soc. 106, 447–462. https://doi.org/10.1002/qj.49710644905, 1980.

Giles, D. M., Sinyuk, A., Sorokin, M. G., Schafer, J. S., Smirnov, A., Slutsker, I., Eck, T. F., Holben, B. N., Lewis, J. R., Campbell, J. R., Welton, E. J., Korkin, S. V., and Lyapustin, A. I.: Advancements in the Aerosol Robotic Network (AERONET) Version 3 database– automated near-real-time quality control algorithm with improved cloud screening for Sun photometer aerosol optical depth (AOD) measurements, Atmos. Meas. Tech., 12, 169 209, https://doi.org/10.5194/amt-12-169-2019, 2019.

Gui, Y., Wang, K., Jin, Z., Wang, H., Deng, H., Li, X., Tian, X., Wang, T., Chen, W., Wang, T., and Piao, S.: The decline in tropical land carbon sink drives high atmospheric CO2 growth rate in 2023, Natl. Sci. Rev., nwae365, https://doi.org/10.1093/nsr/nwae365, 2024.

Hirsch, E. and Koren, I.: Record-breaking aerosol levels explained by smoke injection into the stratosphere, Science, 371, 1269–1274, https://doi.org/10.1126/science.abe1415, 2021.

Hu, Y., Yue, X., and Tian, C.: Climatic drivers of the Canadian wildfire episode in 2023, Atmospheric and Oceanic Science Letters, 17, 100483, https://doi.org/10.1016/j.aosl.2024.100483, 2024.

Huang, H.-Y., Wang, S.-H., Huang, W.-X., Lin, N.-H., Chuang, M.-T., da Silva, A. M., and Peng, C.-M.: Influence of Synoptic-Dynamic Meteorology on the Long-Range Transport of Indochina Biomass Burning Aerosols, J. Geophys. Res.-Atmos., 125, e2019JD031260, https://doi.org/10.1029/2019JD031260, 2020.

Huang, H.-Y., Wang, S.-H., Lau, W.K.M., Wang, S.-Y.S., and da Silva, A.M.: Impact of regional climate patterns on the biomass burning emissions and transport over Peninsular Southeast Asia, 2000–2019. Atmos. Res. 297, 107067. https://doi.org/10.1016/j.atmosres.2023.107067, 2024.

IPCC: Climate Change 2021 – The Physical Science Basis: Working Group I Contribution to the Sixth Assessment Report of the Intergovernmental Panel on Climate Change, Cambridge University Press, Cambridge, https://doi.org/10.1017/9781009157896, 2023.

Formatted: No underline, Font color: Auto

Formatted: No underline, Font color: Auto

Formatted: Font: Not Bold

Formatted: Font: Not Bold

Formatted: No underline, Font color: Auto

Formatted: No underline, Font color: Auto

Jain, P., Barber, Q. E., Taylor, S. W., Whitman, E., Castellanos Acuna, D., Boulanger, Y., Chavardès, R. D., Chen, J., Englefield, P., Flannigan, M., Girardin, M. P., Hanes, C. C., Little, J., Morrison, K., Skakun, R. S., Thompson, D. K., Wang, X., and Parisien, M.-A.: Drivers and impacts of the record-breaking 2023 wildfire season in canada, Nature Communications, 15, 6764, https://doi.org/10.1038/s41467-024-51154-7, 2024.

Jones, M. W., Kelley, D. I., Burton, C. A., Di Giuseppe, F., Barbosa, M. L. F., Brambleby, E., Hartley, A. J., Lombardi, A., Mataveli, G., McNorton, J. R., Spuler, F. R., Wessel, J. B., Abatzoglou, J. T., Anderson, L. O., Andela, N., Archibald, S., Armenteras, D., Burke, E., Carmenta, R., Chuvieco, E., Clarke, H., Doerr, S. H., Fernandes, P. M., Giglio, L., Hamilton, D. S., Hantson, S., Harris, S., Jain, P., Kolden, C. A., Kurvits, T., Lampe, S., Meier, S., New, S., Parrington, M., Perron, M. M. G., Qu, Y., Ribeiro, N. S., Saharjo, B. H., San-Miguel-Ayanz, J., Shuman, J. K., Tanpipat, V., van der Werf, G. R., Veraverbeke, S., and Xanthopoulos, G.: State of Wildfires 2023–2024, Earth Syst. Sci. Data, 16, 3601–3685, https://doi.org/10.5194/essd-16-3601-2024, 2024.

Ke, P., Ciais, P., Sitch, S., Li, W., Bastos, A., Liu, Z., Xu, Y., Gui, X., Bian, J., Goll, D. S., Xi, Y., Li, W., O'Sullivan, M., Goncalves De Souza, J., Friedlingstein, P., and Chevallier, F.: Low latency carbon budget analysis reveals a large decline of the land carbon sink in 2023, National Science Review, 11, nwae367, https://doi.org/10.1093/nsr/nwae367, 2024.

Kim, M.-H., Omar, A. H., Tackett, J. L., Vaughan, M. A., Winker, D. M., Trepte, C. R., Hu, Y., Liu, Z., Poole, L. R., Pitts, M. C., Kar, J., and Magill, B. E.: The CALIPSO version 4 automated aerosol classification and lidar ratio selection algorithm, Atmos. Meas. Tech., 11, 6107–6135, https://doi.org/10.5194/amt11-6107-2018, 2018.

Kolden, C. A., Abatzoglou, J. T., Jones, M. W., and Jain, P.: Wildfires in 2023, Nat. Rev. Earth Environ., 5, 238–240, https://doi.org/10.1038/s43017-024-00544-y, 2024.

Lai, G. and Zhang Y.: Increased atmospheric aridity and reduced precipitation drive the 2023 extreme wildfire season in Canada. Geophy. Res. Lett., 52, e2024GL114492. https://doi.org/10.1029/2024GL114492, 2025.

Liao, Z. H., Ling, Z. H., Gao, M., Sun, J. R., Zhao, W., Ma, P. K., Quan, J. N., and Fan, S. J.: Tropospheric Ozone Variability Over Hong Kong Based on Recent 20 years (2000–2019) Ozonesonde Observation, J. Geophys. Res.-Atmos., 126, https://doi.org/10.1029/2020jd033054, 2021.

Lemus-Canovas, M., Insua-Costa, D., Trigo, R. M., and Miralles, D. G.: Record-shattering 2023 Spring heatwave in western Mediterranean amplified by long-term drought, npj Climate and Atmospheric Science, 7, 25, https://doi.org/10.1038/s41612-024-00569-6, 2024.

Lee, C.-T., Ram, S. S., Nguyen, D. L., Chou, C. C., Chang, S.-Y., Lin, N.-H., Chang, S.-C., Hsiao, T.-C., Sheu, G.-R., and Ou-Yang, C.-F.: Aerosol chemical profile of near-source biomass burning smoke in Sonla, Vietnam during 7-SEAS campaigns in 2012 and 2013, Aerosol Air Qual. Res., 16, 2603–2617, 2016.

Formatted: Font: Not Bold

Formatted: No underline, Font color: Auto

Formatted: No underline, Font color: Auto

Formatted: Font: Not Bold

Lin, N.-H., Tsay, S.-C., Maring, H. B., Yen, M.-C., Sheu, G.-R., Wang, S.-H., Chi, K. H., Chuang, M.-T., Ou-Yang, C.-F., Fu, J. S., Reid, J. S., Lee, C.-T., Wang, L.-C., Wang, J.-L., Hsu, C. N., Sayer, A. M., Holben, B. N., Chu, Y.-C., Nguyen, X. A., Sopajaree, K., Chen, S.-J., Cheng, M.-T., Tsuang, B.-J., Tsai, C.-J., Peng, C.-M., Schnell, R. C., Conway, T., Chang, C.-T., Lin, K.-S., Tsai, Y. I., Lee, W.-J., Chang, S.-C., Liu, J.-J., Chiang, W.-L., Huang, S.-J., Lin, T.-H., and Liu, G.-R.: An overview of regional experiments on biomass burning aerosols and related pollutants in Southeast Asia: From BASE-ASIA and the Dongsha Experiment to 7-SEAS, Atmos. Environ., 78, 1–19, https://doi.org/10.1016/j.atmosenv.2013.04.066, 2013.

Lin, C.-Y., Hsu, H.-M., Lee, Y. H., Kuo, C. H., Sheng, Y.-F., and Chu, D. A.: A new transport mechanism of biomass burning from Indochina as identified by modeling studies, Atmos. Chem. Phys., 9, 7901–7911, https://doi.org/10.5194/acp-9-7901-2009, 2009.

Lin, C. C., Chen, W. N., Loftus, A. M., Lin, C. Y., Fu, Y. T., Peng, C. M., and Yen, M. C.: Influences of the long-range transport of biomass-burning pollutants on surface air quality during 7-SEAS field campaigns, Aerosol Air Qual. Res., 17, 2595–2607, https://doi.org/10.4209/aaqr.2017.08.0273, 2017.

Li, J. Li X. and Ying T.: North Atlantic and the Barents Sea variability contribute to the 2023 extreme fire season in Canada. Proc. Natl Acad. Sci. USA, 121 (49). https://doi.org/10.1073/pnas.241424112, 2024.

Liu, H., Jacob, D. J., Chan, L. Y., Oltmans, S. J., Bey, I., Yantosca, R. M., Harris, J. M., Duncan, B. N., and Martin, R. V.: Sources of tropospheric ozone along the Asian Pacific Rim: An analysis of ozonesonde observations, J. Geophys. Res., 107, ACH 3-1-ACH 3-19, https://doi.org/10.1029/2001JD002005, 2002.

Liu, Z., Deng, Z., Davis, S. J., and Ciais, P.: Global carbon emissions in 2023, Nature Reviews Earth and Environment, 1–2, https://doi.org/10.1038/s43017-024-00532-2, 2024.

Lyu, Y., Wang, J., Zhi, X., Wang, X., Zhang, H., Wen, Y., Park, E., Lee, J., Wan, X., Zhu, S., Dung, D.T.: The characterization, mechanism, predictability, and impacts of the unprecedented 2023 Southeast Asia heatwave. npj Clim. Atmos. Sci. 7, 246. https://doi.org/10.1038/s41612-024-00797-w, 2024.

Ma, T., Chen, W., Cai, Q., Dong, Z., Wang, L., Hu, P., Gao, L., Garfinkel, C.: Attribution analysis of the persistent and extreme drought in Southwest China during 2022–2023. Environ. Res. Lett. https://doi.org/10.1088/1748-9326/ad8171, 2024.

MacCarthy, J., Tyukavina, A., Weisse, MJ., Harris, N., & Glen, E., Extreme wildfires in Canada and their contribution to global loss in tree cover and carbon emissions in 2023. Global Change Biology, 30, e17392. doi:10.1111/gcb.17392, 2024.

McMillan, W. W., Barnet, C., Strow, L., Chahine, M. T., McCourt, M. L., Warner, J. X., Novelli, P. C., Korontzi, S., Maddy, E. S., and Datta, S.: Daily global maps of carbon monoxide from

Formatted: No underline, Font color: Auto

Formatted: No underline, Font color: Auto

Formatted: No underline, Font color: Auto

Formatted: No underline, Font color: Auto

Formatted: No underline, Font color: Auto

Formatted: No underline, Font color: Auto

NASA's Atmospheric Infrared Sounder, Geophys. Res. Lett., 32, L11801, https://doi.org/10.1029/2004GL021821, 2005.

McMillan, W. W., Evans, K. D., Barnet, C. D., Maddy, E. S., Sachse, G. W., and Diskin, G. S.: Validating the AIRS Version 5 CO retrieval with DACOM in situ measurements during INTEX-A and -B, IEEE T. Geosci. Remote, 49, 2802–2813, https://doi.org/10.1109/TGRS.2011.2106505, 2011.

Michailidis, K., Garane, K., Karagkiozidis, D., Peletidou, G., Voudouri, K.-A., Balis, D., and Bais, A.: Extreme wildfires over northern Greece during summer 2023 – Part A: Effects on aerosol optical properties and solar UV radiation, Atmospheric Research, 311, 107700, https://doi.org/10.1016/j.atmosres.2024.107700, 2024.

Min, S. K.: Human influence can explain the widespread exceptional warmth in 2023. *Commun. Earth Environ.* 5, 215 https://doi.org/10.1038/s43247-024-01391-x, 2024.

Omar, A. H., Winker, D. M., Vaughan, M. A., Hu, Y., Trepte, C. R., Ferrare, R. A., Lee, K.-P., Hostetler, C. A., Kittaka, C., Rogers, R. R., Kuehn, R. E., and Liu, Z.: The CALIPSO automated aerosol classification and lidar ratio selection algorithm, J. Atmos. Ocean. Tech., 26, 1994–2014, https://doi.org/10.1175/2009JTECHA1231.1, 2009.

Ou-Yang, C. F., Lin, N. H., Sheu, G. R., Lee, C. T., and Wang, J. L.: Seasonal and diurnal variations of ozone at a high-altitude mountain baseline station in East Asia, Atmos. Environ., 46, 279–288, https://doi.org/10.1016/j.atmosenv.2011.09.060, 2012.

Ou-Yang, C. F., Lin, N. H., Lin, C. C., Wang, S. H., Sheu, G. R., Lee, C. Te, Schnell, R. C., Lang, P. M., Kawasato, T., and Wang, J. L.: Characteristics of atmospheric carbon monoxide at a high-mountain background station in East Asia, Atmos. Environ., 89, 613–622, https://doi.org/10.1016/j.atmosenv.2014.02.060, 2014.

Ou-Yang, C. F., Ravindra Babu, S., Lee, J.-R., Yen, M.-C., Griffith, S. M., Lin, C.-C., Chang, S.-C., and Lin, N.-H.: Detection of stratospheric intrusion events and their role in ozone enhancement at a mountain background site in sub-tropical East Asia, Atmos. Environ., 268, 118779, https://doi.org/10.1016/j.atmosenv.2021.118779, 2022.

Pani, S. K., Wang, S. H., Lin, N. H., Lee, C. Te, Tsay, S. C., Holben, B. N., Janjai, S., Hsiao, T. C., Chuang, M. T., and Chantara, S.: Radiative effect of springtime biomass-burning aerosols over northern Indochina during 7-SEAS/BASELInE 2013 campaign, Aerosol Air Qual. Res., 16, 2802–2817, https://doi.org/10.4209/aaqr.2016.03.0130, 2016.

Pani, S. K., Ou-Yang, C.-F., Wang, S.-H., Ogren, J. A., Sheridan, P. J., Sheu, G.-R., and Lin, N.-H. J. A. E.: Relationship between long-range transported atmospheric black carbon and carbon monoxide at a high-altitude background station in East Asia, Atmos. Environ, 210, 86–99, https://doi.org/10.1016/j.atmosenv.2019.04.053, 2019.

Formatted: Font: Not Bold

Formatted: Font: Not Bold

Formatted: No underline, Font color: Auto

Formatted: No underline, Font color: Auto

Pani, S.K., Huang, H.-Y., Wang, S.-H., Holben, B.N., Lin, N.-H.: Long-term observation of columnar aerosol optical properties over the remote South China Sea. Sci. Total Environ. 905, 167113 https://doi.org/10.1016/j.scitotenv.2023.167113, 2023.

Platnick, S., King, M. and Hubanks, P.: MODIS Atmosphere L3 Monthly Product. https://doi.org/10.5067/MODIS/MOD08_M3.006, 2015.

Perkins-Kirkpatrick, S., Barriopedro, D., Jha, R., Wang, L., Mondal, A., Libonati, R., and Kornhuber, K.: Extreme terrestrial heat in 2023, Nature Reviews Earth & Environment, 5, 244–246, https://doi.org/10.1038/s43017-024-00536-y, 2024.

Raghuraman, S. P., Soden, B., Clement, A., Vecchi, G., Menemenlis, S., and Yang, W.: The 2023 global warming spike was driven by the El Niño–Southern Oscillation, Atmos. Chem. Phys., 24, 11275–11283, https://doi.org/10.5194/acp-24-11275-2024, 2024.

Ramanathan, V., Crutzen, P. J., Kiehl, J. T., and Rosenfeld, D.: Aerosols, climate, and the hydrological cycle, Science, 294, 2119–2124, https://doi.org/10.1126/science.1064034, 2001.

Ravindra Babu, S., Ou-Yang, C.-F., Griffith, S. M., Pani, S. K., Kong, S. S.-K., and Lin, N.-H.: Transport pathways of carbon monoxide from Indonesian fire pollution to a subtropical high-altitude mountain site in the western North Pacific, Atmos. Chem. Phys., 23, 4727–4740, https://doi.org/10.5194/acp-23-4727-2023, 2023.

Ravindra Babu, S. and Lin, N-H.: Changing pattern of springtime biomass burning over Peninsular Southeast Asia (PSEA) in recent decades. ESS Open Archive . August 08, 2023. DOI: 10.22541/essoar.169111389.92212046/v2, 2023.

Reid, J. S., Hyer, E. J., Johnson, R., Holben, B. N., Yokelson, R. J., Zhang, J., Campbell, J. R., Christopher, S. A., Di Girolamo, L., Giglio, L., Holz, R. E., Kearney, C., Miettinen, J., Reid, E. A., Turk, F. J., Wang, J., Xian, P., Zhao, G., Balasubramanian, R., Chew, B. N., Janai, S., Lagrosas, N., Lestari, P., Lin, N.-H., Mahmud, M., Nguyen, A. X., Norris, B., Oahn, N. T. K., Oo, M., Salinas, S. V., Welton, E. J., Liew, S. C.: Observing and understanding the Southeast Asian aerosol system by remote sensing: An initial review and analysis for the Seven Southeast Asian Studies (7SEAS) program, Atmos. Res., 122, 403–468, https://doi.org/10.1016/j.atmosres.2012.06.005, 2013.

Roy, D. P., De Lemos, H., Huang, H., Giglio, L., Houborg, R. and Miura, T.: Multi-resolution monitoring of the 2023 Maui wildfires, implications and needs for satellite-based wildfire disaster monitoring. *Sci. Remote Sens.* 10, 100142. https://doi.org/10.1016/j.srs.2024.100142, 2024.

Sayer, A. M., Munchak, L. A., Hsu, N. C., Levy, R. C., Bettenhausen, C., and Jeong, M. J..: MODIS collection 6 aerosol products: comparison between Aqua's e-Deep Blue, Dark Target, and "merged" datasets, and usage recommendations, J. Geophys. Res. Atmos., 119, 13965–13989, 2014.

Formatted: No underline, Font color: Auto

Formatted: No underline, Font color: Auto

Formatted: No underline, Font color: Auto

Formatted: No underline, Font color: Auto

Formatted: No underline, Font color: Auto

Formatted: Font: Not Bold

Formatted: Font: Not Bold

Formatted: No underline, Font color: Auto

Formatted: No underline, Font color: Auto

Seneviratne, S. I., Zhang, X., Adnan, M., Badi, W., Dereczynski, C., Di Luca, A., Ghosh, S., Iskandar, I., Kossin, J., Lewis, S., Otto, F., Pinto, I., Satoh, M., Vicente-Serrano, S. M., Wehner, M., and Zhou, B.: Weather and Climate Extreme Events in a Changing Climate. In Proc. *Climate Change 2021: The Physical Science Basis*. Contribution of Working Group I to the Sixth Assessment Report of the Intergovernmental Panel on Climate Change, 1513–1766 (Cambridge University Press, 2021). https://doi.org/10.1017/9781009157896.013, 2021

Sheu, G.-R., Lin, N.-H., Wang, J.-L., Lee, C.-T., Ou Yang, C.-F., and Wang, S.-H.: Temporal distribution and potential sources of atmospheric mercury measured at a high-elevation background station in Taiwan, Atmos. Environ., 44, 2393–2400, https://doi.org/10.1016/j.atmosenv.2010.04.009, 2010.

Sinyuk, A., Holben, B. N., Eck, T. F., Giles, D. M., Slutsker, I., Korkin, S., Schafer, J. S., Smirnov, A., Sorokin, M., and Lyapustin, A.: The AERONET Version 3 aerosol retrieval algorithm, associated uncertainties and comparisons to Version 2, Atmos. Meas. Tech., 13, 3375–3411, https://doi.org/10.5194/amt 13-3375-2020, 2020.

Torbenson, M. and Büntgen, U.: summer warmth unparalleled over the past 2,000 years. *Nature* 631, 94–97 (2024). https://doi.org/10.1038/s41586-024-07512-y, 2023.

Tsay, S. C., Maring, H. B., Lin, N. H., Buntoung, S., Chantara, S., Chuang, H. C., Gabriel, P. M., Goodloe, C. S., Holben, B. N., Hsiao, T. C., Christina Hsu, N., Janjai, S., Lau, W. K. M., Lee, C. Te, Lee, J., Loftus, A. M., Nguyen, A. X., Nguyen, C. M., Pani, S. K., Pantina, P., Sayer, A. M., Tao, W. K., Wang, S. H., Welton, E. J., Wiriya, W., and Yen, M. C.: Satellitesurface perspectives of air quality and aerosol-cloud effects on the environment: An overview of 7-SEAS/BASELInE, Aerosol Air Qual. Res., 16, 2581–2602, https://doi.org/10.4209/aaqr.2016.08.0350, 2016.

Twomey, S.: The Influence of Pollution on the Shortwave Albedo of Clouds, Journal of Atmospheric Sciences, 34, 1149–1152, https://doi.org/10.1175/1520-0469(1977)034<1149:TIOPOT>2.0.CO;2, 1977.

Wang, S., Guan, L., Cohen, J.B., and Qin, K.: Reconstructing top-down global black carbon emissions using remote sensing and models, Atmospheric Pollution Research, 16, 10, (102633). https://doi.org/10.1016/j.apr.2025.102633, 2025.

Wang, S., Cohen, J. B., Deng, W., Qin, K., and Guo, J.: Using a New Top-Down Constrained Emissions Inventory to Attribute the Previously Unknown Source of Extreme Aerosol Loadings Observed Annually in the Monsoon Asia Free Troposphere, Earths Fut., 9, e2021EF002167, https://doi.org/10.1029/2021EF002167, 2021.

Wang, S., Cohen, J. B., Guan, L., Lu, L., Tiwari, P., & Qin, K.: Observationally constrained global NOx and CO emissions variability reveals sources which contribute significantly to CO2 emissions, npj Climate and Atmospheric Science, 10.1038/s41612-025-00977-2, 8, 1, 2025.

Warner, J. X., Comer, M. M., Barnet, C. D., McMillan, W. W., Wolf, W., Maddy, E., and Sachse, G.: A Comparison of Satellite Tropospheric Carbon Monoxide Measurements from AIRS and

Formatted: No underline, Font color: Auto

Formatted: No underline, Font color: Auto

Formatted: Font: Not Bold

Formatted: No underline, Font color: Auto

Formatted: No underline, Font color: Auto

Formatted: Font: Not Bold

Formatted: No underline, Font color: Auto

MOPITT During INTEX-A, J. Geophys. Res., 112, D12S17, https://doi.org/10.1029/2006JD007925, 2007.

Warner, J., Carminati, F., Wei, Z., Lahoz, W., and Attié, J.-L.: Tropospheric carbon monoxide variability from AIRS under clear and cloudy conditions, Atmos. Chem. Phys., 13, 12469–12479, https://doi.org/10.5194/acp-13-12469-2013, 2013.

Wai, K. M., Lin, N., Wang, S., and Dokiya, Y.: Rainwater chemistry at a high-altitude station, Mt. Lulin, Taiwan: Comparison with a background station, Mt. Fuji, J. Geophys. Res.-Atmos., 113, D06305, https://doi.org/10.1029/2006JD008248, 2008.

Wei, J., Li, Z., Peng, Y., and Sun, L.: MODIS Collection 6.1 aerosol optical depth products over land and ocean: validation and comparison, Atmos. Environ., 201, 428–440, 2019a.

Wei, J., Li, Z., Sun, L., Peng, Y., and Wang, L.: Improved merge schemes for MODIS Collection 6.1 Dark Target and Deep Blue combined aerosol products, Atmos. Environ., 202, 315–327, 2019b.

Worden, H., Deeter, M., Edwards, D., Gille, J., Drummond, J., and Nédélec, P.: Observations of near-surface carbon monoxide from space using MOPITT multispectral retrievals, J. Geophys. Res.-Atmos., 115, D18314, https://doi.org/10.1029/2010JD014242, 2010.

Xia, L., Liu, R., Fan, W., and Ren, C.: Emerging carbon dioxide hotspots in East Asia identified by a top-down inventory, Commun. Earth Environ., 6, 1–13, https://doi.org/10.1038/s43247-024-01991-7, 2025.

Yadav, I. C., Linthoingambi Devi, N., Li, J., Syed, J. H., Zhang, G., and Watanabe, H.: Biomass burning in Indo-China peninsula and its impacts on regional air quality and global climate change – a review, Environ. Pollut., 227, 414–427, https://doi.org/10.1016/j.envpol.2017.04.085, 2017.

Zachariah, M., Vautard, R., Chaithra, S. T., Kimutai, J., Arulalan, T., AchutaRao, K., Otto, F. E. L.: Extreme humid heat in South and Southeast Asia in April 2023, largely driven by climate change, detrimental to vulnerable and disadvantaged communities. World Weather Attribution. https://doi.org/10.25561/104092, 2023.

Zeng, Z. and Sun, J.: Impacts of a tripolar sea surface temperature pattern over tropical–North Pacific on interannual variations of spring extreme consecutive dry days over southern China. J. Geophys. Res. Atmos. 127, e2021JD036281. https://doi.org/10.1029/2021JD036281, 2022.

Formatted: No underline, Font color: Auto

Formatted: No underline, Font color: Auto

Formatted: No underline, Font color: Auto

Formatted: No underline, Font color: Auto